Assortative mixing in micro-architecturally annotated brain connectomes

Vincent Bazinet[1], Justine Y. Hansen[1], Reinder Vos de Wael[1],
Boris C. Bernhardt[1], Martijn P. van den Heuvel[2], Bratislav Misic[1]*
[1]*McConnell Brain Imaging Centre, Montréal Neurological Institute, McGill University, Montréal, Canada*
[2]*Center for Neurogenomics and Cognitive Research, Vrije Universiteit Amsterdam, Amsterdam, Netherlands*

The wiring of the brain connects micro-architecturally diverse neuronal populations. The conventional graph model encodes macroscale brain connectivity as a network of nodes and edges, but abstracts away the rich biological detail of each regional node. Regions are different in terms of their microscale attributes, many of which are readily available through modern technological advances and data-sharing initiatives. How is macroscale connectivity related to nodal attributes? Here we investigate the systematic arrangement of white-matter connectivity with respect to multiple biological annotations. Namely, we formally study assortative mixing in annotated connectomes by quantifying the tendency for regions to be connected with each other based on the similarity of their micro-architectural attributes. We perform all experiments using four cortico-cortical connectome datasets from three different species (human, macaque and mouse), and consider a range of molecular, cellular and laminar annotations, including gene expression, neurotransmitter receptors, neuron density, laminar thickness and intracortical myelin. Importantly, we disentangle the relationship between neural wiring, regional heterogeneity and spatial embedding using spatial autocorrelation-preserving null models. We show that mixing between micro-architecturally diverse neuronal populations is supported by long-distance connections. Using meta-analytic decoding, we find that the arrangement of connectivity patterns with respect to biological annotations shape patterns of regional functional specialization. Specifically, regions that connect to biologically similar regions are associated with executive function; conversely, regions that connect with biologically dissimilar regions are associated with memory function. By bridging scales of cortical organization, from microscale attributes to macroscale connectivity, this work lays the foundation for next-generation annotated connectomics.

Keywords: brain networks | connectome | cytoarchitectonics | neurotransmitter receptors | transcriptomics

INTRODUCTION

The brain is a complex network of anatomically connected and functionally interacting neuronal populations [16]. Representing the brain as a graph of grey matter nodes interconnected by white matter edges allows us to articulate and quantify its organizational principles. A compact set of hallmark features has been documented across organisms, spatial scales and reconstruction technologies [92]. These include communities of densely interconnected brain regions and disproportionately well connected hubs [84, 94]. Together, these features promote a balance between specialization and integration [83].

An important limitation of the graph model of the brain is the assumption that all regions are the same. Yet, regions differ in their intrinsic micro-architectural attributes [45, 48, 88, 89, 108]. These attributes include gene expression [18, 28, 32, 33, 43, 50], cellular morphology [77, 95] and density [21], cell type [78], neurotransmitter receptor profiles [30, 38, 42, 66], laminar differentiation [59, 67, 105, 107], and myelination [47]. Understanding how the heterogeneous micro-architectural attributes of regional nodes are related to their connectional fingerprint is a fundamental question in systems neuroscience [51, 69, 89, 102].

Multiple studies have shown that the arrangement of connections and regional attributes are related. For example, regions with more macroscale connections tend to have more dendritic spines, larger dendritic trees and greater neural density [77]. Moreover, regions with similar attributes are more likely to be connected with each other [13, 32, 42, 47, 80, 107], suggesting a tendency for homophilic attachment. However, the assessment of the relationship between connectivity and micro-architecture is complicated by the background influence of the brain's spatial embedding on both, whereby spatially proximal regions are likely to have similar micro-architecture, but also to share anatomical connections [46, 58, 74, 87]. Disentangling the relationships between neural wiring, regional heterogeneity and spatial embedding is a core challenge [1, 65]. Furthermore, studies are often limited to a constrained set of attributes in a single organism, precluding discovery of universal principles of cortico-cortical organization.

Here we apply principled methods from network science to construct annotated connectomes. We use connectomes reconstructed from tract-tracing in model organisms as well as high-resolution *in vivo* imaging in humans, and annotate them with multiple micro-architectural attributes including gene expression, neuron density, receptor fingerprints and intracortical myelin. We then systematically quantify the assortativity of these annotated connectomes: the tendency of regions with similar attributes to connect with one an-

* Corresponding author: bratislav.misic@mcgill.ca

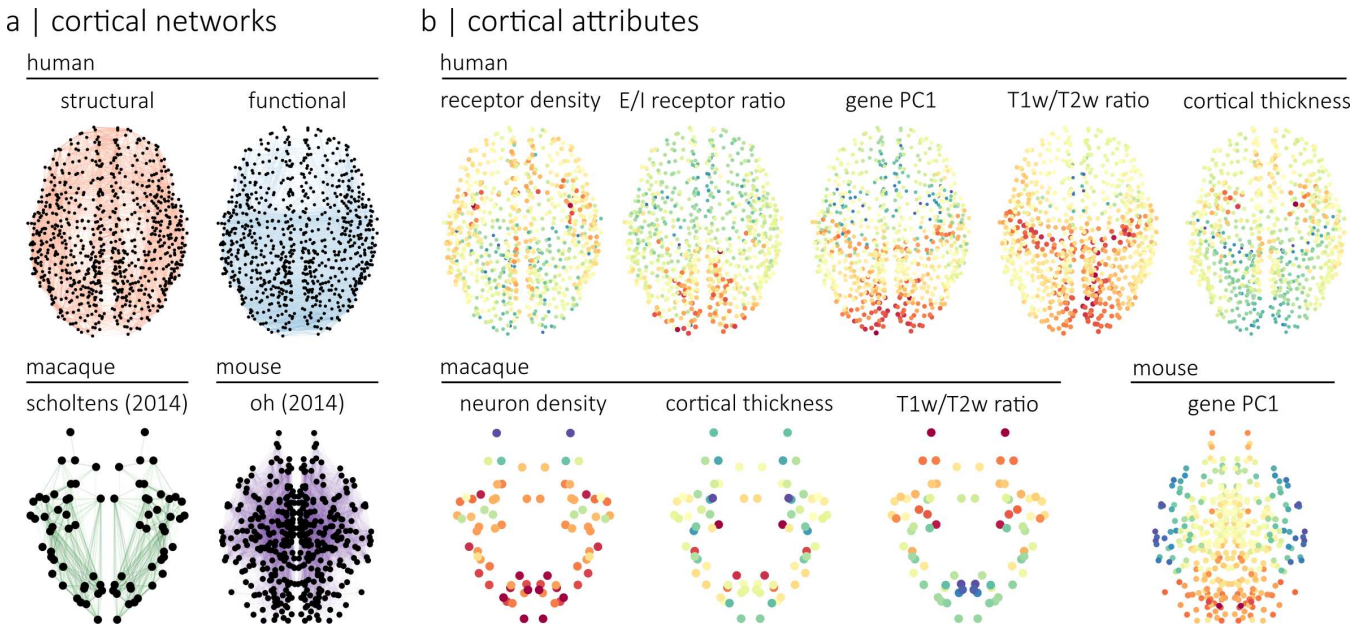

Figure 1. **Annotated connectomes** | We annotated four connectomes with micro-architectural attributes. **(a)** Connectomes include a human structural and a human functional connectome reconstructed using data from the HCP [98], a macaque connectome generated using data from the CoCoMac database and initially introduced in Scholtens et al. [77], and a mouse connectome reconstructed using data from the Allen Mouse Brain Connectivity Atlas and introduced in Oh et al. [64]. **(b)** Human connectomes are annotated with measures of neurotransmitter receptor density, the ratio of excitatory-to-inhibitory neurotransmitter receptors, the principal axis of gene expression (gene PC1), T1w/T2w ratio and cortical thickness. The macaque connectome is annotated with neuron density (neuron-to-cell ratio), cortical thickness and T1w/T2w ratio. The mouse connectome is annotated with the principal axis of gene expression (gene PC1).

other. In particular, we implement a novel null model to assess the contribution of spatial constraints. We find a tendency for regions with similar annotations to connect with each other, and highlight the role of long-distance projections in connecting micro-architecturally diverse regions. We also generalize the concept of assortative mixing to address two biologically relevant questions about wiring principles of brain networks. First, we consider heterophilic assortativity: are regions enriched with one attribute more likely to be connected with regions enriched with another attribute? Second, we consider local assortativity: how similar is a region to its connected neighbors in terms of its annotations?

RESULTS

The results are organized as follows. We first use the assortativity coefficient to explore the relationship between connectivity and the regional distribution of nodal attributes. We then specifically look at the assortative mixing of long-range connections. Finally, we uncover heterophilic patterns of connectivity between different micro-architectural properties and extend the general concept of assortativity to the local level.

We use four different connectomes, namely a human diffusion-weighted MRI structural connectome, a human resting-state functional MRI connectome, a macaque tract-tracing connectome and a mouse tract-tracing connectome (Fig. 1a). Each connectome is annotated with micro-architectural annotations. In other words, each node in the connectome is given a local annotation score associated with a micro-architectural attribute. The human connectomes are annotated with cortical thickness, T1w/T2w ratio (a proxy for intra-cortical myelin [36]), the ratio of excitatory-to-inhibitory neurotransmitter receptors in a region (E/I ratio), the density of neurotransmitter receptors in a region and the principal axis of gene expression (gene PC1). The macaque is annotated with cortical thickness, T1w/T2w ratio and neuron density while the mouse connectome is annotated with its principal axis of gene expression (Fig. 1b).

Assortativity of cortical attributes

We first explore the relationship between micro-architectural annotations and connectome organization using the assortativity coefficient. For a given annotated network, assortativity is defined as the Pearson correlation between the local annotation scores of connected nodes [63]. In other words, it quantifies the tendency for nodes with similar annotation scores to be connected (Fig. 2a). An important challenge for measuring assortativity is that cortical attributes are spatially autocorrelated, and at the same time, connections also tend to

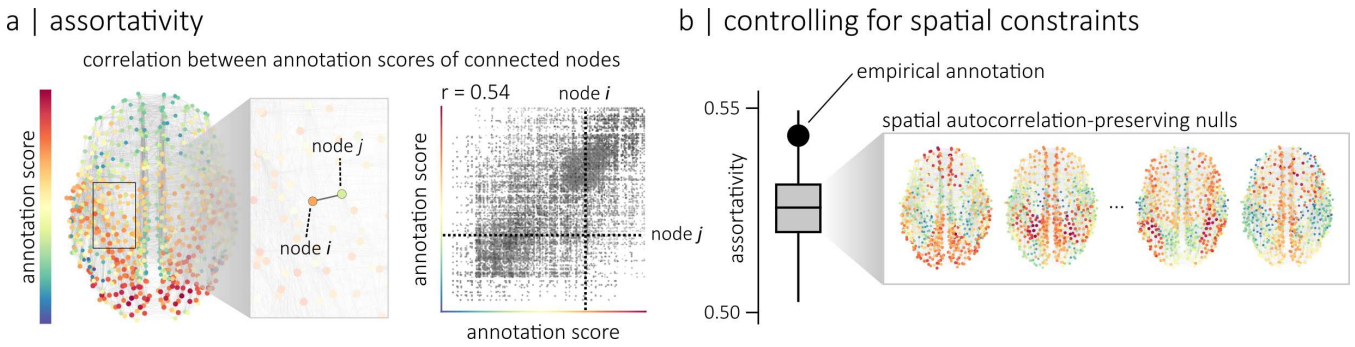

Figure 2. **Assortative mixing | (a)** Given an annotated network where each node has a local annotation score, we can quantify the tendency for nodes with similar scores to be connected using the assortativity coefficient. This coefficient is defined as the Pearson correlation between the scores of connected nodes [63]. This relationship between the scores of connected nodes can be visualized with a scatterplot of a network's edges where the position of each edge is determined by the annotation scores of its two endpoints. Here, the intersection of the two dashed lines indicates the position of the edge highlighted in the zoomed-in frame of the network. In this example, the assortativity coefficient (r) is equal to 0.54. **(b)** To control for spatial constraints, the assortativity coefficient of an empirical annotation can be compared to the assortativity coefficients of null annotations that preserve the spatial autocorrelation of the empirical one [2, 19, 58].

form between brain regions that are proximal in space [87]. As a result, assortativity may be trivially confounded by spatial embedding. To assess how cortical attributes are related to brain connectivity, we control for this spatial autocorrelation [2, 19, 58]. Namely, we compare empirical assortativity coefficients to the assortativity coefficients of null annotations with preserved spatial autocorrelation (Fig. 2b).

We find that all annotations are positively assortative (i.e. brain regions tend to be connected to other regions with similar attributes), but that surrogate annotations also have positive assortativity scores (Fig. 3a). To account for the influence of spatial autocorrelation on assortativity, we compute the standardized assortativity score (z-assortativity) of each attribute relative to the null distributions of spatial autocorrelation-preserving surrogates (Fig. 3b). We find that annotations are not significantly assortative on the human structural connectome, while gene PC1 (z-assort$= 2.31, p_{\text{spin}} = 0.0142$), T1w/T2w (z-assort$= 5.51, p_{\text{spin}} < 0.0001$) and cortical thickness (z-assort$= 3.21, p_{\text{spin}} = 0.0015$) are significantly assortative on the human functional connectome. In the macaque connectome, we observe a significant difference between the assortativity of T1w/T2w and null annotations (z-assort$= 3.95, p_{\text{moran}} = 0.0005$) as well as between neuron density and null annotations (z-assort$= 3.98, p_{\text{moran}} < 0.0001$). No such significant difference is observed for the cortical thickness. In the mouse connectome, no significant difference is observed for gene PC1. To ensure that the results are not sensitive to our processing choices, we also replicated our experiments using different parcellation schemes, single-hemisphere connectomes, an independently acquired dataset and additional spatially-autocorrelation preserving nulls models (Figs. S1, S2, S3).

Our results show that there are numerous instances where annotations that are *prima facie* assortative are actually not significantly assortative when we account for spatial autocorrelation. We do find instances, however, where assortativity is significantly larger than expected from the brain's spatial embedding and, interestingly, these findings are consistent with recent reports in the literature. The significant standardized assortativity of neuron density in the macaque cortex is consistent with reports that neuron density is more related to the existence of connections than geodesic distance [14]. Significant assortativity in the functional connectome is also consistent with recent reports that functional connectivity gradients are closely aligned with multiple micro-architectural properties [18, 47, 48, 67].

Geometric contributions to assortativity

Recent theories suggest that long-distance connections in the structural connectome enhance the diversity of a brain region's inputs and outputs [11]. Long-distance connections may thus potentially promote communication between regions with dissimilar attributes. This idea, however, has never been formally tested from the perspective of biological annotations.

We therefore explored how the standardized assortativity of different attributes, relative to null annotations with preserved spatial auto-correlation, varies as we consider connections of different lengths. For all four connectomes and for each annotation, we compute the standardized assortativity across thresholded connectomes where a given percentile of the shortest connections is removed. We find that as short-distance connections are removed — leaving behind the longest connections — the standardized assortativity of all annotations across all four connectomes decreases (Fig. 4). Notably, with 75% of the human structural connectome's connections

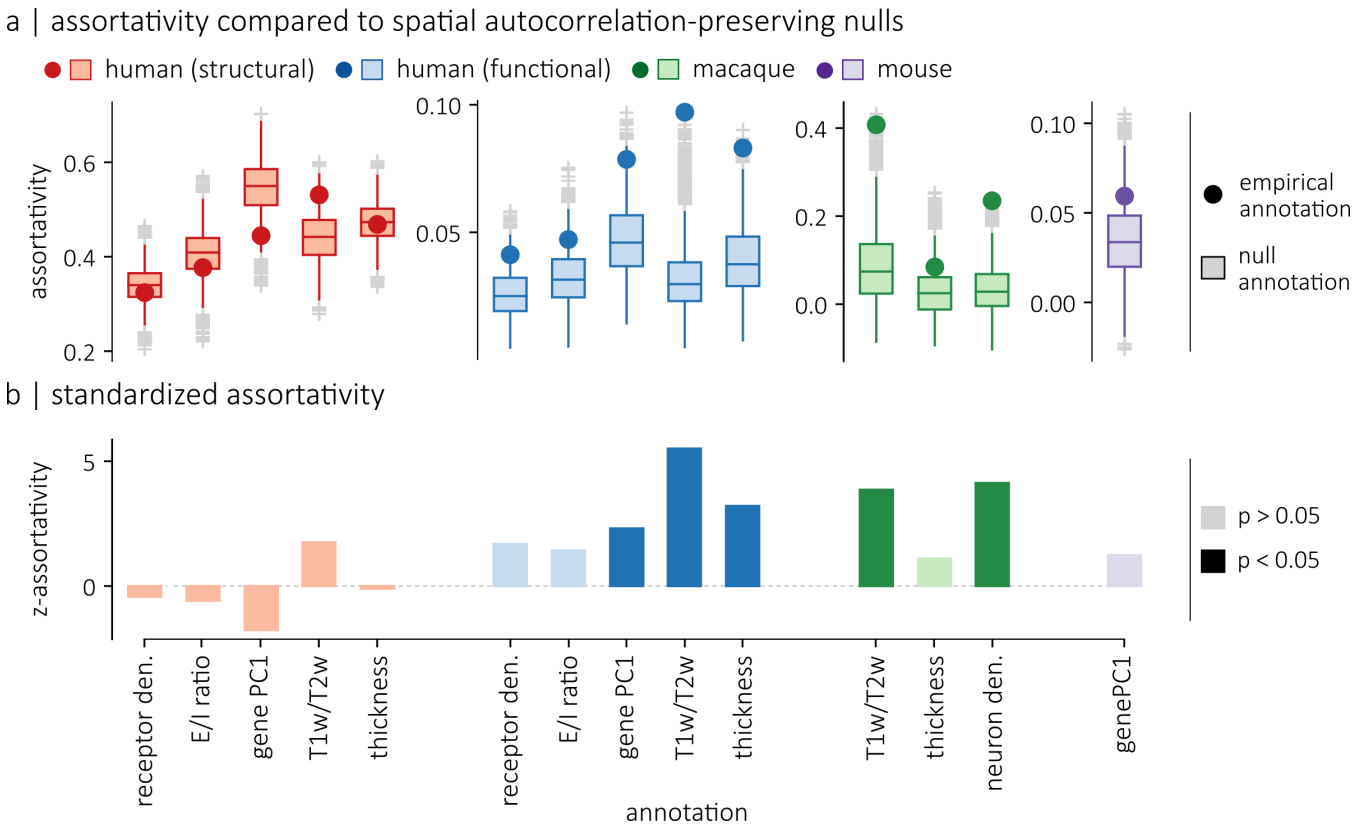

Figure 3. **Standardized assortativity of micro-architectural annotations | (a)** Assortativity of empirical annotations are compared to null annotations with preserved spatial autocorrelation. For the human connectomes, the nulls were generated using a spatial permutation model. For the mouse and macaque connectomes, the nulls were generated using a parameterized null model. **(b)** Standardized assortativity scores (z-assortativity), computed relative to the spatial autocorrelation-preserving null annotations. Gene PC1 (p_{spin}=0.0142), T1w/T2w ratio (p_{spin}<0.0001) and cortical thickness (p_{spin}=0.0015) are significantly assortative on the functional connectome, while T1w/T2w (p_{moran}=0.0005) and neuron density (p_{moran}<0.0001) are significantly assortative on the macaque connectome.

removed, all five annotations become significantly disassortative. In other words, the remaining long-range connections link regions with attributes that are more dissimilar than we would expect from the brain's spatial embedding. Again, these results are consistent across multiple methodological choices (Figs. S1, S2, S3). This confirms the notion that long-distance connections increase the diversity of a region's inputs and outputs, supporting the integration of information between micro-architecturally dissimilar regions.

Heterophilic mixing of cortical attributes

In the previous sections, we used the assortativity coefficient to ask if two areas are more likely to be connected if they are enriched with the same attribute. In other words, we quantified the homophilic mixing of micro-architectural attributes. An equally important question is whether there exists heterophilic mixing in the brain. In other words, are two regions more likely to be connected if one region is enriched with one attribute while the other is enriched with a different attribute? Cortico-cortical connectivity may indeed reflect interactions between pairs of distinct attributes. For instance, it has been hypothesised that the noradrenergic and cholinergic systems influence in distinct ways large-scale dynamical processes in the brain [81]. Laminar organization also appears to be closely related to brain connectivity [34, 39, 75]. We next ask if the heterogeneous distribution of pairs of attributes from multi-member classes of annotation — neurotransmitter receptor profiles and laminar differentiation — is reflected in the connectivity of the brain.

To address these questions, we analyze two datasets (Fig. 5a). The first is a positron emission tomography (PET)-derived atlas of 18 receptors and transporters from 9 neurotransmitter systems [42]. The second is the thickness of individual cortical layers in the Merker-stained BigBrain histological atlas [3, 105]. To quantify heterophilic mixing, we extend the concept of assortativity to pairs of annotations. In other words, we compute the assortativity coefficient for pairs of annotations

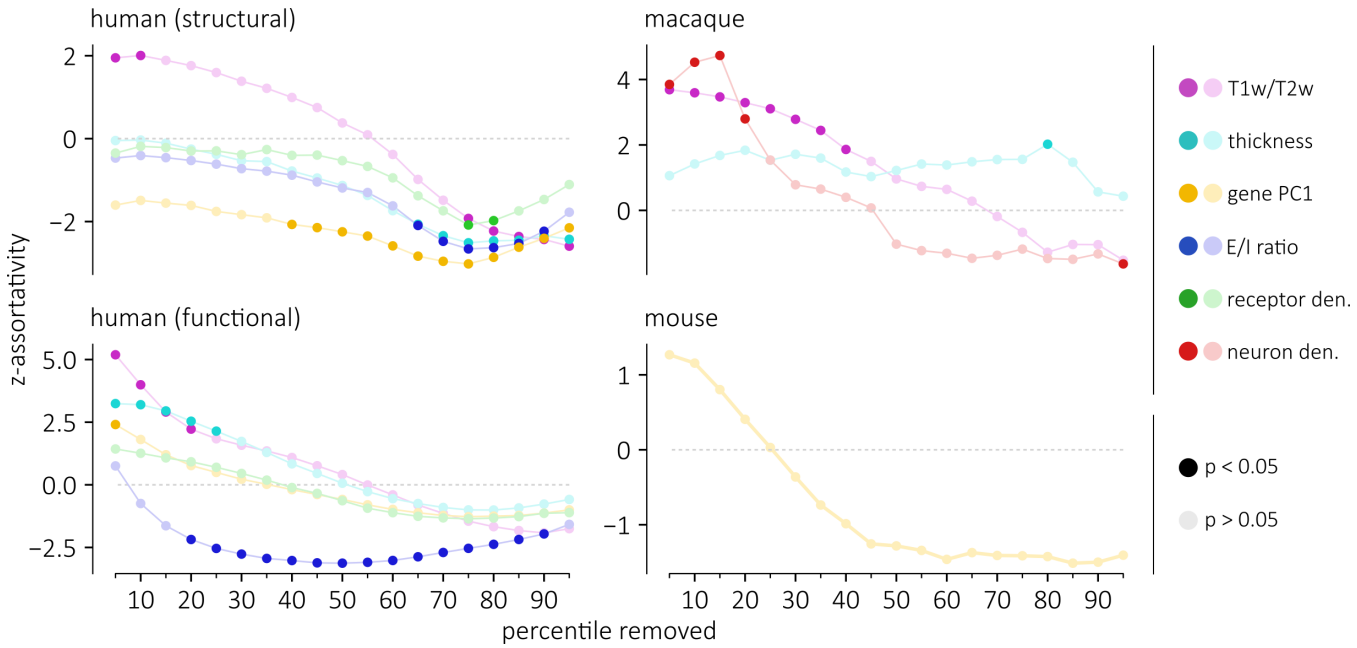

Figure 4. **Assortative mixing of long-range connections |** Assortativity is computed in each of the four connectomes, thresholded such that a percentile of the shortest connections are removed. These assortativity scores are standardized with respect to a null distribution of spatial autocorrelation-preserving nulls. Standardized assortativity scores (z-assortativity) for each annotation are displayed as a function of the percentile of connections removed in the network. For all four connectomes, annotations become less assortative as short-range connections are removed.

such that the annotation at endpoint i represents an attribute $\mathbf{x}$ and the annotation at endpoint j represents a different attribute $\mathbf{y}$. Fig. 5b shows the heterophilic mixing matrices of the structural and functional connectomes for both receptor density and laminar thickness. The assortativity results are standardized with respect to spatial autocorrelation-preserving null annotations generated by permuting the attributes on the surface of the brain (spins). Importantly, these permutations preserve the correlation between brain maps. By controlling for both the brain's spatial embedding and the correlation between brain maps, our analyses specifically assess the relationship between brain connectivity and the heterogeneous distributions of pairs of micro-architectural attributes. Positive values in each matrix indicate that a region that scores highly on an annotation $\mathbf{x}$ is more likely to be connected to a region that scores highly on an annotation $\mathbf{y}$ than expected from the spatial distribution of each annotation. Negative values indicate that a region that scores high on an annotation $\mathbf{x}$ is more likely to be connected to a region that scores low on an annotation $\mathbf{y}$ than expected from the spatial distribution of each annotation.

Several salient associations emerge that are consistent with prior intuitions and qualitative descriptions in the literature (Fig. 5b). For the functional connectome, we find that layer IV is significantly disassortative with layers III (z-assort$= -2.41, p_{\text{spin}} = 0.02$), V (z-assort$= -2.15, p_{\text{spin}} = 0.03$) and VI (z-assort$= -2.21, p_{\text{spin}} = 0.03$). In other words, brain areas with a prominent layer IV are less likely to be connected to areas that have prominent layers III, V and VI than what would be expected from the topographic organization of laminar thickness gradients. Importantly, layer IV is most prominent in the primary visual cortex, while the thicknesses of layers III, V and VI increase along the sensory processing hierarchy [105]. This result therefore supports the idea that microscale attributes and macroscale functional connectivity are predominantly arranged along a core organizing axis from sensory to higher-order association brain regions [48].

This general idea also extends to receptors where we broadly find evidence of disassortative mixing for pairs of receptors that are predominantly expressed in brain regions on opposite ends of the processing hierarchy. For instance, we find disassortative mixing between the noradrenaline transporter (NAT), and the serotonergic 5HT2a receptors (SC: z-assort$= -2.86, p_{\text{spin}} = 0.0077$; FC: z-assort$= -6.06, p_{\text{spin}} < 0.0001$). This is in line with the cortical distribution of these receptors; namely, NAT has the greatest density in motor cortex [42], while 5HT2a has the greatest density in the primary visual cortex [111]. We also find a significant assortative relationship between vesicular acetylcholine transporters (VaChT) and NAT (SC: z-assort$= 2.21, p_{\text{spin}} = 0.0279$; FC: z-assort$= 4.85, p_{\text{spin}} = 0.0002$). Transporters are generally expressed pre-synaptically. Thus, our results show that regions densely innervated by cholinergic neurons

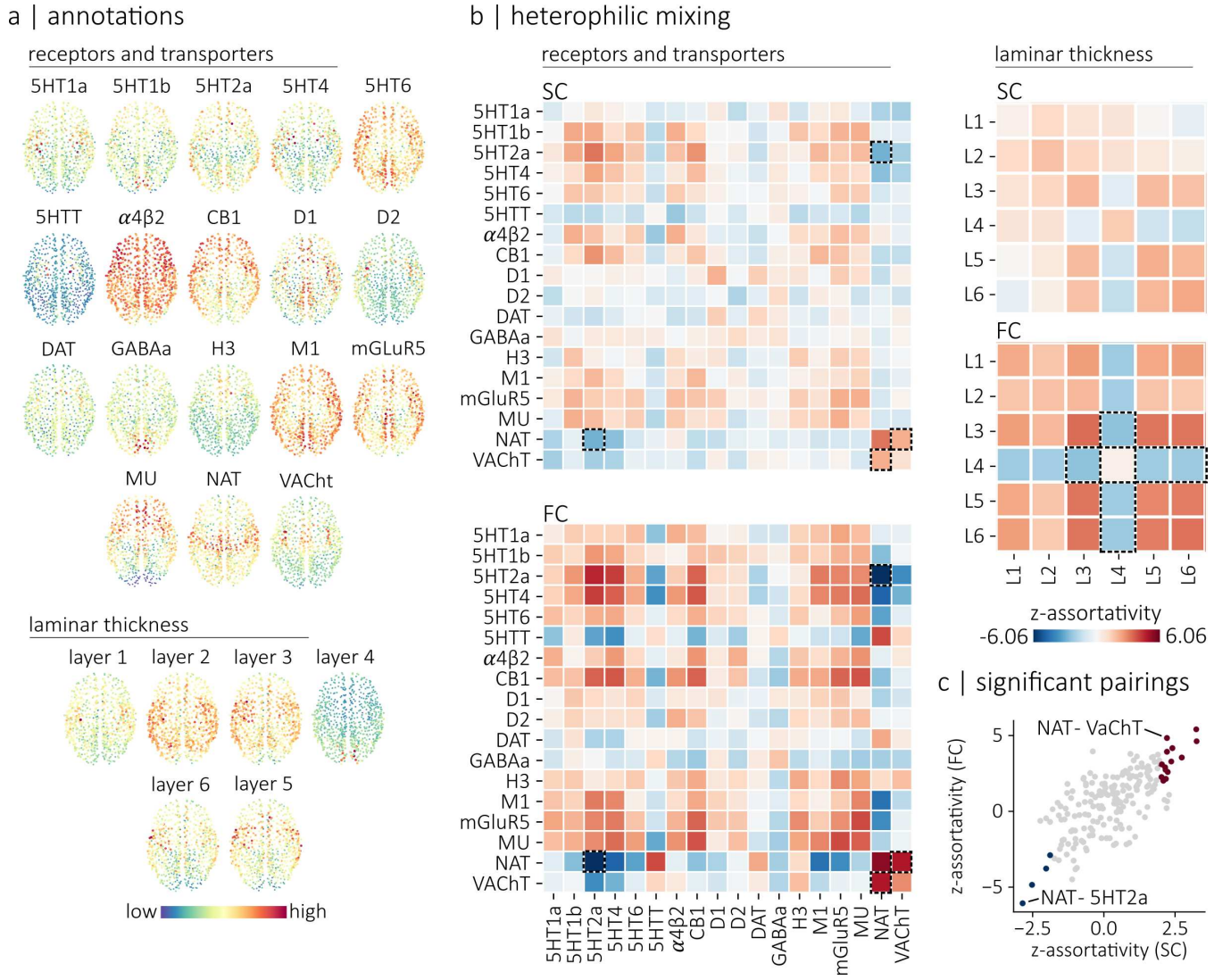

Figure 5. **Heterophilic mixing | (a)** Topographic distribution of PET-derived brain maps showing the density of 18 transporters and receptors [42], as well as the topographic distribution of laminar thicknesses extracted from the Merker-stained BigBrain histological atlas [3, 105] **(b)** Heterophilic mixing matrices for the receptors/transporter annotations (left) and for the laminar thickness annotations (right). Positive values indicate that regions that score highly on an annotation $\mathbf{x}$ are more likely to be connected to regions that score highly on an annotation $\mathbf{y}$ than would be expected from the brain's spatial embedding. Negative values indicate that regions that score high on an annotation $\mathbf{x}$ are more likely to be connected to regions that score low on an annotation $\mathbf{y}$. Dashed squares highlight specific examples of assortative and disassortative heterophilic relationships: the significantly disassortative relationship between the noradrenaline transporter (NAT), and the serotonergic 5HT2a receptors (SC: z-assort$= -2.86, p_{\text{spin}} = 0.0077$; FC: z-assort$= -6.06, p_{\text{spin}} < 0.0001$), the significantly assortative relationship between vesicular acetylcholine transporters (VaChT) and NAT (SC: z-assort$= 2.21, p_{\text{spin}} = 0.0279$; FC: z-assort$= 4.85, p_{\text{spin}} = 0.0002$) as well as the disassortative relationships between layer IV thickness and layers III, V and VI. **(c)** Relationship between the standardized assortativity of annotation pairs in the structural connectome (SC) and in the functional connectome (FC). We find a strong relationship between z-assortativity in SC and z-assortativity in FC (r=0.69). Highlighted in red are annotation pairs that are significantly assortative in both SC and FC. Highlighted in blue are annotation pairs that are significantly disassortative in both SC and FC.

tend to be connected, both structurally and functionally, with regions densely innervated by noradrenaline neurons, above and beyond what would be expected from the brain's spatial embedding. Our findings therefore support the idea that these two systems interact with each other and with the brain's topology to influence large-scale dynamical processes [81]. Assortative relationships tend to be similar in both structural and functional connectomes (Fig. 5c). They are also replicable with alternate parcellations and datasets (Fig. S4).

Collectively, these complex heterophilic mixing patterns show evidence of how macroscale white matter projections support interfacing among neuronal populations with diverse microscale attributes.

Local assortative mixing

In the previous two sections, we explored how cortical attributes align with the underlying connectome at the global level. Here we extend this concept to the local level and consider the extent to which individual regions connect to regions with similar attributes. We first compute the absolute difference between the local annotation scores of connected nodes (Fig. 6a, left). To quantify the local assortativity of a region, we then compute the weighted average of its annotation differences to its connected neighbours, weighted by the connection weight between the two nodes (nodal mean difference; Fig. 6a, right). This local assortativity score represents how different a region is from other regions it is anatomically connected with in terms of its biological attributes.

Importantly, annotation scores that deviate from the mean are on average more dissimilar to other scores (Fig. 6b). To account for this, we define the homophilic ratio of a node as the ratio between its nodal mean difference with connected neighbors and the average absolute difference between its annotation score and the annotation scores of all the other nodes in the network (Fig. 6b). Nodes that have large homophilic ratios are nodes that tend to connect to brain regions with more dissimilar properties (disassortative) while nodes that have small homophilic ratios tend to connect to regions with more similar properties (assortative).

The homophilic ratios of all five annotations on the structural connectome are shown in Fig. 6c. The homophilic ratios are consistent across parcellations and datasets (Fig. S6). We also computed the homophilic ratio of each annotation on the functional connectome (Fig. S5). For the structural connectome, we summarized the assortativity of each node by computing their averaged homophilic ratio across all five annotations and quantified the relationship between homophilic ratio and mean connection distance as well as node strength (Fig. 6d). We find a significant relationship for both mean connection distance (r=0.36, $p_{\text{spin}} = 0.0001$), and node strength (r=0.27, $p_{\text{spin}} = 0.003$). In other words, disassortative regions have, on average, longer connections, which is consistent with our previous findings that long distance connections tend to be disassortative (Fig. 4). Also, our finding that disassortative regions have larger node strength suggests that "hub" nodes that are more central in the network tend to have more diverse connectivity profiles.

Finally, we ask whether the homophilic ratio of a brain region shapes its functional specialization. We extracted brain maps of probabilistic associations between functional keywords and individual voxels using the Neurosynth meta-analytic engine [109] and correlated the brain maps associated with 123 cognitive and behavioural terms [70] with the averaged homophilic ratios. We find significant negative correlations ($p_{\text{spin}} < 0.05$) between average homophilic ratio and terms associated with higher-order executive functions (e.g. planning, working memory, intelligence; Fig. 6e, right) and significant positive correlations between the average homophilic ratio brain map and terms associated with information consolidation and memory (e.g. sleep, semantic memory and navigation; Fig. 6e, left). This suggests that executive functions are subtended by a network of areas that tend to connect to other areas with similar microscale attributes. Conversely, integrative functions such as consolidation and memory are subtended by a set of medial temporal structures that project to regions with diverse microscale attributes.

DISCUSSION

In the present report we investigate the link between connectome architecture and microscale biological annotations. More specifically, we ask whether brain regions with similar attributes are more likely to be connected with each other above and beyond the role of spatial proximity. We systematically assess the tendency for global and local homophilic mixing across a variety of attributes. We show that mixing between microarchitecturally diverse neuronal populations is supported by long-distance connections. Finally, we highlight how brain connectivity supports heterophilic mixing patterns between neurotransmitter systems and cortical layers.

The present work builds upon an exciting new direction in network neuroscience to jointly consider macroscale networks and microscale attributes [51, 65, 77, 88, 95]. Contemporary theories emphasize the link between cytoarchitectonic similarity and synaptic connectivity [6, 34, 39, 44, 75]. Numerous recent reports related macroscale connectivity to microscale annotations, including gene expression [5, 29, 32, 73, 101], cytoarchitecture [13, 14, 47, 67, 107] and neurotransmitter receptor profiles [30, 42]. While some of these studies have shown evidence of global assortative mixing for specific attributes and connectomes types, the extent to which these findings can be generalized to wiring principles across network reconstruction techniques, species, spatial scales and annotations remains unknown. By considering a broad range of annotation in multiple connectome datasets, the present work comprehensively studies how connectivity between neural populations depends on their micro-architecture.

Importantly, the spatial embedding of the brain constrains its organization [87]. Microscale attributes are graded across the cortex [48, 57, 89], which means that most cortical attributes are spatially autocorrelated [18, 19, 31, 58]. There is also a concomitant prevalence of short-distance connections compared to long-distance connections [17], with connection probability and strength typically decaying exponentially with spa-

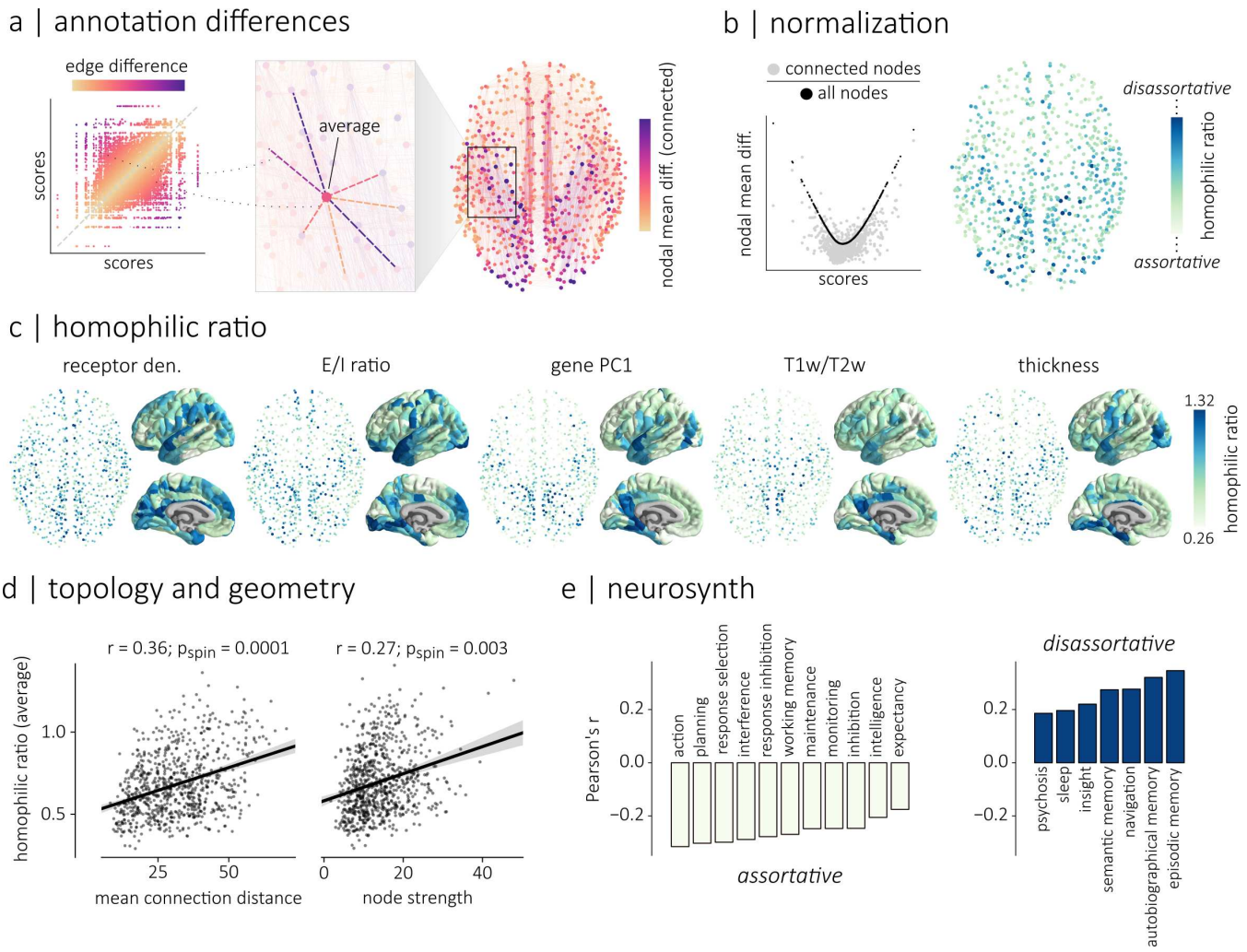

Figure 6. **Local assortative mixing |** We quantified the assortative properties of individual brain regions. **(a)**. For each brain region, we computed the weighted average of the absolute differences between its local annotation score and the local annotation scores (nodal mean differences) of its directly-connected neighbors. **(b)** Annotation scores that deviate from the mean of the distribution are on average more dissimilar to other scores. This can be shown with a scatterplot of the relationship between nodal mean difference and annotation score. The average absolute difference between a node's annotation score and the annotation scores of all the other nodes in the network (black points) is directly related to its annotation score. We see a similar relationship if we only consider connected neighbors (gray points). A node's homophilic ratio is therefore defined as its nodal mean difference with connected neighbors, divided by the average of the differences between its annotation score and the annotation scores of all the nodes in the network. Nodes with large homophilic ratios tend to connect to brain regions with dissimilar properties (disassortative) while nodes with small homophilic ratios tend to connect to other regions with similar properties (assortative). **(c)** Homophilic ratios, for the human structural connectome, are shown for five micro-architectural attributes. **(d)** Homophilic ratio averaged across the five micro-architectural attributes shown in panel c, is compared to the mean connection distance of a node (right) and to nodal strength (left). We find significant relationships between homophilic ratio and both measures (mean connection distance: r=0.36, $p_{\text{spin}} = 0.0001$; nodal strength: r=0.27, $p_{\text{spin}} = 0.003$. **(e)** We correlated 123 parcellated brain maps of probabilistic associations between functional keywords and individual voxel activation [109] with the average homophilic ratio of each node. We find 11 significantly positive relationships and 7 significantly negative relationships ($p_{\text{spin}} < 0.05$). Brain maps that are significantly and positively related to homophilic ratio are associated to functional keywords related to executive functions (e.g. planning, working memory, intelligence). In other words, regions that show large activation during these tasks tend to have a small homophilic ratio and therefore tend to be connected to regions with similar microscale attributes. Brain maps that are significantly but negatively related to homophilic ratio are associated to functional keywords related to memory and integrative functions (e.g. insight, semantic memory, episodic memory, navigation). In other words, regions that show large activation during these tasks tend to have diverse connectivity profiles.

tial distance [27, 37, 46, 61, 74]. Collectively, these principles of cortical organization necessitate careful consideration and methodological control of spatial effects when studying the relationship between connectivity and annotations [2, 18, 19, 31, 58, 99].

Here, we rigorously assess how network wiring, microarchitectural features and spatial embedding are intertwined from the perspective of assortativity. Although degree assortativity – whether nodes with similar degrees are more likely to be connected with each other – has previously been studied in brain networks [8, 9, 41, 62, 96], the fundamental idea is more general and can be applied to any nodal features. In this sense, assortativity, combined with spatially-constrained null models, is the ideal framework to study connectome annotations.

For the functional connectome, we find a significant relationship between connectivity and gene PC1, T1w/T2w and cortical thickness. This is consistent with previous reports that these three properties are related to the principal gradient of functional connectivity [18, 47, 48], which can be thought of as the dominant pattern of "assortativity" in functional connectomes [55]. For the structural connectome, we find that assortative connectivity heavily depends on the annotation itself. While we find significant assortativity in the macaque for T1w/T2w and neuron density (consistent with previous reports [14]), we find also numerous counter-examples of annotations that are not assortative beyond the background effect of spatial embedding. For instance, we find that receptor density and E/I ratio, T1w/T2w ratio, cortical thickness and gene PC1 are not assortative in the human connectome, nor is gene PC1 assortative on the mouse connectome. Collectively, these results support a general tendency for cytoarchitectonically similar regions to be connected, but also highlight the fact that not all features conform to this wiring principle.

By definition, assortativity means that brain regions will be connected to regions that are similar to themselves; a functional consequence is that regions are less likely to be exposed to diverse inputs. Importantly, we find that long distance connections are an architectural feature that potentially serves to diversify inputs to a brain region. Indeed, the longest connections, in structural (diffusion and tract-tracing) and functional connectomes are significantly disassortative, meaning that they are more likely to connect dissimilar regions than expected from the brain's spatial embedding. This is in line with the notion that greater prevalence of short-range connections [27, 37, 46, 61, 74], which presumably entail lower material and metabolic cost [17], is counterbalanced by a small number of high-cost, high-benefit long-range connections that support communication between regions with diverse functions [10, 53]. Previous studies have found that long-range connections, which are heterogeneously distributed along microarchitectural and cognitive hierarchies [79, 106], help to shorten communication pathways [94], and bridge specialized modules [11]. Our results build on this literature by showing that long-range connections are also more likely to be placed between regions that are biologically distinct.

We also extend the conventional framework of assortativity to ask two biologically important questions about heterophilic and local homophilic mixing. The notion of heterophilic mixing becomes particularly convenient when we study a multi-member class of annotations, and wish to know whether a node enriched with one attribute is likely to be connected to a node enriched with another attribute. In the brain, two notable examples are receptor profiles and laminar differentiation, both of which have been associated to patterns of synaptic connectivity [39, 42]. For instance, ascending cholinergic and noradrenergic neuromodulatory systems are thought to provide complementary mechanisms to balance segregation (cholinergic) and integration (noradrenergic) [81]. Our results highlight a tendency for cortical areas that are rich in cholinergic and noradrenergic transporters to be connected, offering a potential anatomical mechanism to maintain this balance. We also find that the thickness of granular layer IV, which is more prominent in sensory regions, is disassortative with the thickness of the other layers of the cortex. This is in line with previous findings that have shown that sensory regions, such as visual cortex, form segregated modules in macroscale structural and functional networks [41, 60, 72, 110]. How heterophilic mixing is organized between different classes (e.g. areas enriched with specific layers connected to areas enriched with specific receptors [111]) remains an exciting question that could be readily addressed with the present framework.

Finally, we "zoom in" to specific regions and assess the extent to which their local biological annotations conform to the annotations of their connected neighbours, thereby generalizing the concept of global assortativity to the local level. Using meta-analytic decoding, we find that regions that connect to biologically similar regions tend to be associated with executive function. This may reflect the fact that these areas (e.g. dorsolateral prefrontal cortex), which are cytoarchitecturally distinct from other prefrontal regions [7], form a highly interconnected module in the structural connectome [41]. Conversely, regions that connect with biologically dissimilar regions tend to be associated with memory function. This may reflect the idea that these regions (e.g. medial temporal cortex) are involved in integrating signals from multiple specialized circuits [62]. Collectively, these results show that the arrangement of connectivity patterns with respect to biological annotations may ultimately shape patterns of regional functional specialization.

The present results should be interpreted with respect to important methodological limitations. First, human structural connectomes were reconstructed using diffusion imaging, a technique that is known to yield multiple false positives and false negatives [54, 90], and which cannot be used to infer directionality. Although we replicated the results using high fidelity tract-tracing

and histology in multiple animal models, further development in reconstructing human white-matter connectomes is needed. Second, although we tried to be as extensive and comprehensive as possible in our choice of annotations, spanning molecular, cellular and laminar attributes, the final set is obviously incomplete. Exciting technological and data-sharing advances will eventually permit even more detailed and comprehensive biological annotations to be studied using this framework. Relationship between connectivity and attributes depend on how brain regions are defined (i.e. parcellations). We systematically studied multiple parcellations, but how best to delineate functional territories of the cortex remains an open challenge in the field [15, 26].

In summary, the present work bridges scales of cortical organization, from microscale attributes to macroscale connectivity. By carefully controlling the background effect of spatial embedding, we systematically assess how connectivity is interdigitated with a broad range of micro-architectural attributes and empirically test multiple theories about the wiring of cortical networks. This work lays the foundation for next-generation annotated connectomics.

METHODS

Connectomes

Human connectomes (HCP)

The human connectomes were generated using data from the Human Connectome Project S900 release [98]. Scans from N=201 unrelated participants were used to reconstruct a consensus structural and functional connectome. Informed consent was obtained for all subjects (the protocol was approved by the Washington University Institutional Review Board as part of the HCP). The participants were scanned in the HCP's custom Siemens 3T "Connectome Skyra" scanner, and the acquisition protocol included a high angular resolution imaging (HARDI) sequence and four resting state fMRI sessions. Briefly, the dMRI data was acquired with a spin-echo EPI sequence (TR=5,520 ms; TE=89.5 ms; FOV=210 $\times$ 180 mm^2; voxel size=1.25 mm^3; b-value=three different shells i.e., 1,000, 2,000, and 3,000 s/mm^2; number of diffusion directions=270; and number of b0 images=18) and the resting-state fMRI data was acquired using a gradient-echo EPI sequence (TR=720 ms; TE=33.1 ms; FOV=208×180 mm^2; voxel size=2 mm^3; number of slices=72; and number of volumes=1,200). Additional information regarding the acquisition protocol is available at [98].

The data was pre-processed according to the HCP minimal preprocessing pipelines [35] and structural connectomes were reconstructed from the dMRI data using the MRtrix3 package [91]. Grey matter was parcellated into 800 cortical regions according to the Schaefer functional atlas [76] and fiber orientation distributions were generated using a multi-shell multi-tissue constrained spherical deconvolution algorithm [24, 49]. The initial tractogram was generated with 40 million streamlines, with a maximum tract length of 250 and a fractional anisotropy cutoff of 0.06. Spherical-deconvolution informed filtering of tractograms (SIFT2) was used to reconstruct whole brain streamlines weighted by cross-section multipliers [82]. More information regarding the individual network reconstructions is available at [68].

A group consensus structural network was then built such that the mean density and edge length distribution observed across individual participants was preserved [12]. The weights of the edges in the consensus networks correspond to the log-transform of the number of streamlines in the parcels, averaged across participants for whom these edges existed. A group-average functional connectivity matrix was constructed by concatenating the regional fMRI BOLD time series of all four resting-state sessions from all participants and computing the zero-lag Pearson correlation coefficient between each pair of brain regions. To threshold this matrix, we generated 1000 bootstrapped connectivity matrices by randomly sampling 276 points from the concatenated time series and by computing the correlation between these pairs of bootstrapped time series. Using these bootstrapped samples, we then estimated confidence intervals and retained the correlations between pairs of regions that were consistently positive or negative. Inconsistent correlations were set to 0. Experiments were also replicated using connectomes parcellated into 400 cortical regions, again according to the Schaefer functional atlas [76], and without log-transforming the edge weights.

Human connectomes (Lausanne)

Our experiments were also replicated in a second dataset collected at the Lausanne University Hospital ($N = 67$; age 28.8 $\pm$ 9.1 years, 40% females) [40]. Participants were scanned in a 3-Tesla MRI Scanner (Trio, Siemens Medical, Germany). Informed consent was obtained for all subjects (the protocol was approved by the Ethics Committee of Clinical Research of the Faculty of Biology and Medicine, University of Lausanne, Switzerland). Details regarding data acquisition, preprocessing and network reconstruction are available at [40]. Briefly, the data acquisition protocol included a magnetization-prepared rapid acquisition gradient echo (MPRAGE) sequence (1mm in-plane resolution, 1.2mm slice thickness), a diffusion spectrum imaging (DSI) sequence (128 diffusion-weighted volumes and a single b0 volume, maximum b-value 8,000 s/mm^2, 2.2 $\times$ 2.2 $\times$ 3.0 mm voxel size), and a gradient echo-planar imaging (EPI) sequence sensitive to blood-oxygen-level-dependent (BOLD) contrast (3.3 mm in-plane resolution and slice thickness with a 0.3-mm gap, TR 1,920 ms, resulting in 280 images per participant). Grey matter

was parcellated into either 219 and 1000 equally sized parcels [20]. The Connectome Mapper Toolkit was used for the initial signal processing [22] while gray and white matter were segmented from the MPRAGE volume using freesurfer [23]. Structural connectivity matrices were reconstructed for individual participants using deterministic streamline tractography on reconstructed DSI data. 32 streamline propagations were initiated per diffusion direction and per white matter voxel.

Again, a group consensus structural network was built such that the mean density and edge length distribution observed across individual participants was preserved [12]. The weights of the edges correspond to the log-transform of the streamline densities, averaged across participants and scaled to values between 0 and 1. fMRI volumes were corrected for physiological variables (regression of white matter, cerebrospinal fluid, as well as motion), BOLD time series were subjected to a lowpass filter and motion "scrubbing" [71] was performed. A group-average functional connectivity matrix was reconstructed using the same procedure as described above.

Macaque connectome

The macaque connectome was initially introduced in Scholtens et al. [77] and was generated using data from the CoCoMac database, an online repository of tract-tracing experiments [86]. The parcellation used for the network reconstruction is an hybrid between the Walker-von Bonin and Bailey atlases [85] and contains 39 non-overlapping cortical regions. The network was constructed such that a connection is assigned to pairs of brain regions if i) a tract is reported in a least five studies in the database and ii) at least 66% of the reports are positive. The connectome is directed and each edge is weighted between 1 and 3 based on the averaged reported strength of the connection.

Mouse connectome

The mouse connectome was generated by Oh et al. [64] using data from the Allen Mouse Brain Connectivity Atlas. This connectivity atlas contains high-resolution images acquired from 469 injection experiments performed in the right hemisphere of C57BL/6J male mice. Each experiment produced 140 high-resolution (0.35μm) coronal sections of EGFP-labelled axonal projections which were then registered to the Allen Mouse Brain Atlas [52]. A weighted directed connectome of 213 brain regions was constructed. The strength of each connection was obtained by fitting a linear connectivity model to the data. The connectivity data, the name of the 213 brain regions as well as the euclidean distance between each region was obtained from the supplemental material of Oh et al. [64]. The spatial coordinates used for visualization were obtained from the Allen Mouse Reference Atlas, version 2 (2011).

Annotations

Human annotations

Cortical thickness and **T1w/T2w ratio** were extracted from high-resolution structural scans made available by the Human Connectome Project [98]. For the HCP connectomes, the morphometric measures were obtained for each one of the 201 individuals used to reconstruct the connectomes and averaged, for each node of the parcellations, across subjects. For the Lausanne connectomes, the morphometric measures, averaged across subjects of the S1200 release, were fetched and parcellated using neuromaps [57].

The principal axis of transcriptional variation across the human cortex (**gene PC1**) was computed using the Allen Human Brain Atlas (AHBA; https://human.brain-map.org/) [43], which provides regional microarray expression data from six post-mortem brains (1 female, ages 24-57, 42.5 ± 13.38). The AHBA data was pre-processed and mapped to the parcellated brain regions using the abagen toolbox (https://github.com/rmarkello/abagen) [56]. During pre-processing, the MNI coordinates of tissue samples were updated to those generated via non-linear alignment to the ICBM152 template anatomy (https://github.com/chrisgorgo/alleninf). Microarray probe information was re-annotated for all genes using data provided by Arnatkeviciute and colleagues [4]. For bilateral connectomes, microarray expression samples were mirrored across hemispheres to increase spatial coverage. Then, probes were filtered by only retaining those that have a proportion of signal to noise ratio greater than 0.5. When multiple probes indexed the expression of the same gene, the one with the most consistent pattern of regional variation across donors was selected. Samples were then assigned to individual regions in the parcellations. If a sample was not found directly within a parcel, the nearest sample, up to a 2mm-distance, was selected. If no samples were found within 2mm of the parcel, the sample closest to the centroid of the empty parcel across all donors was selected. To reduce the potential for misassignment, sample-to-region matching was constrained by hemisphere and gross structural divisions (i.e., cortex, subcortex/brainstem, and cerebellum, such that e.g., a sample in the left cortex could only be assigned to an atlas parcel in the left cortex). All tissue samples not assigned to a brain region in the provided atlas were discarded. Tissue sample expression scores were then normalized across genes using a scaled robust sigmoid function [32], and were rescaled to a unit interval. Expression scores were also normalized across tissue samples using the same procedure. Microarray samples belonging to the same regions were then aggregated by computing the

mean expression across samples for individual parcels, for each donor. Regional expression profiles were finally averaged across donors to obtain a single genes $\times$ brain regions matrix. From the 15,632 genes listed in this matrix, 1,906 brain-specific genes were used to compute the principal axis of transcriptional variation using Principal component analysis. The list of brain-specific genes was obtained from [18].

Receptor density information was collected for 18 different neurotransmitter receptors and transporters from a total of 25 different studies as described in [42]. Positron emission tomography (PET) images registered to the MNI space were parcellated and receptors/transporters with more than one mean image of the same tracer (5-HT1b, D2, VAChT) were combined using a weighted average. Tracer maps, each corresponding to a single receptor/transporter where then normalized across regions to values between 0 and 1. **Receptor density** was computed as the average density, across all 18 receptors while an **excitatory/inhibitory ratio** was computed as the ratio between the mean density of excitatory receptors and the mean density of inhibitory receptors. Excitatory receptors include: 5HT2a, 5HT4, 5HT6, A4B2, D1, M1, mGLuR5. Inhibitory receptors include: 5HT1a, 5HT1b, CB1, D2, GABAa, H3, MU.

Laminar thickness information was extracted from the Merkel-stained BigBrain histological atlas [3, 105]. Individual cortical layers were individually segmented with a convolutional neural network, as described in Wagstyl et al. [105], and the laminar surfaces were made available on the BigBrain Project website (https://ftp.bigbrainproject.org/). Laminar thickness was computed as the Euclidean distance between each pair of corresponding vertices on each 3D surfaces. The data was then parcellated to the Schaefer (800 nodes) parcellation [76] using surface parcellation files in the BigBrain space that are also available on the BigBrain Project website.

Macaque annotations

Three macaque annotations were obtained. The **cortical thickness** and **T1w/T2w ratio** cortical maps are originally from Donahue et al. [25] and were extracted from the structural MRI scans of 19 adult macaques (T1w and T2w, 0.5mm isotropic). These brain maps were publicly shared in the BALSA database [97] (https://balsa.wustl.edu/study/show/W336). The cortical maps were first parcellated using a 91 regions parcellation scheme (M132). The data was then further parcellated to the WBB atlas using a region-wise mapping provided in [93]. **Neuron density** information was extracted from brain tissues of an Old World macaque monkey [21] and mapped to the WBB atlas using a mapping provided in [77].

Mouse annotations

The principal axis of gene expression variation (**gene PC1**) was computed using data from the Allen Mouse Brain Atlas [52]. This atlas contains gene expression profiles, obtained using *in-situ* hybridization, from more than 20,000 genes. Expression density within each of the 213 structures defined in the oh2014 connectome was computed by combining/unionizing grid voxels with the same 3-D structural label. The data was obtained using the mouse module of the abagen toolbox (https://github.com/rmarkello/abagen) [56]. To facilitate comparison between genes, we normalized expression levels for each gene. We then computed the principal axis of gene expression variation across brain regions using principal component analysis.

Spatial autocorrelation-preserving null annotations

We controlled for the brain's spatial constraints using null models that preserve the spatial autocorrelation of the empirical attributes. Three different null models were used. For the human networks, the results presented in the main text relied on a spatial permutation model (spin nulls) [2]. They were also replicated with a parameterized null model that uses Moran spectral randomization (Moran nulls) [103] and with a third null model originally proposed by Burt and colleagues (Burt nulls) [19]. In the animal connectomes, results presented in the main text used the Moran nulls and were replicated using the Burt nulls. The spin, Moran and Burt nulls were respecively implemented with the neuromaps (https://github.com/netneurolab/neuromaps) [57], brainspace (https://github.com/MICA-MNI/BrainSpace) and brainSMASH (https://github.com/murraylab/brainsmash) [19] toolboxes.

Spin nulls

The original framework for this spatial permutation model was introduced in Alexander-Bloch et al. [2] and consists in generating null distributions by applying random rotations to spherical projections of the brain. Here, we use a framework adapted to parcellated data originally proposed in Vázquez-Rodríguez et al. [100]. Namely, we select for each parcel the vertex closest to its center of mass on the spherical projection of the *fsaverage* surface. We then apply a rotation to the coordinates of these centers of mass and reassign to each parcel the value of the closest rotated parcel. To preserve homotopy across hemispheres, the rotations are generated independently for one hemisphere and then mirrored across the anterior-posterior axis for the other. This procedure is repeated 10,000 times.

Moran nulls

The generation of spatially constrained nulls using Moran spectral randomization was first proposed in the ecology literature [104] and relies on a spatially-informed weight matrix $\mathbf{W}$. The eigenvectors of $\mathbf{W}$ provide an estimate of the autocorrelation in the brain and are used to impose a similar spatial structure on random, normally distributed surrogate data. Here, $\mathbf{W}$ is defined as the inverse of the distance matrix between brain regions. For the human connectomes, the distance between pairs of parcels was defined as the mean geodesic distance between every vertex pair in both parcels. In the animal connectomes, it was defined as the euclidean distance between both parcels. Data was generated separately for each hemisphere using the same random seed to obtain null annotations that preserve homotopy across hemispheres.

Burt nulls

This parameterized null model was originally proposed in Burt et al. [19]. First, the empirical brain map is randomly permuted. Then, this permuted brain map is spatially smoothed and re-scaled to re-introduce the spatial autocorrelation (SA) of the empirical brain map. The smoothing process is achieved via the following transformation:

$$\mathbf{y} = |\beta|^{1/2}\,\mathbf{x} + |\alpha|^{1/2}\,\mathbf{z}, \tag{1}$$

where $\mathbf{y}$ is the surrogate map, $\mathbf{x}$ is the permuted data and $\mathbf{z}$ is a vector of random gaussian noise. The α and β parameters are estimated via a least-square optimization between variograms of the original and permuted data. By maximizing the fit between the variograms of the original and permuted data, we ensure that the SA of the surrogate map matches the SA of the empirical map. Again, the distances between pairs of parcels in the human connectomes were obtained by averaging the geodesic distance between every vertex in the two parcels while they were obtained by computing the euclidean distance between each parcel in the animal connectomes. Also, data was generated separately for each hemisphere using the same random seed to obtain null annotations that preserve homotopy across hemispheres. The hyper-parameters used were the default parameters provided by the brainSMASH software [19] (https://github.com/murraylab/brainsmash).

Assortativity

To study the relationship between distributions of cortical attributes and the topological architecture of our connectomes, we relied on the assortativity coefficient, which is defined as the Pearson correlation between the annotations of connected nodes [63]. More precisely, given an adjacency matrix $\mathbf{A}$, where a_{ij} represents the strength of the connection between brain regions i and j, and a vector of annotations $\mathbf{x}$, where x_i represents the annotation attributed to node i, the assortativity of a network, with respect to $\mathbf{x}$ is defined as:

$$r_{\mathbf{x}} = \sum_{ij} \frac{a_{ij}}{2m} \tilde{x_i} \tilde{x_j}, \tag{2}$$

where $2m$ corresponds to the sum of the edge weights in the network and $\tilde{x_i}$ represents the standardized score of the annotation attributed to node i:

$$\tilde{x_i} = \frac{x_i - \bar{\mathbf{x}}}{\sigma_{\mathbf{x}}}, \tag{3}$$

$\bar{\mathbf{x}}$ corresponds to the expected value of $\mathbf{x}$ and $\sigma_{\mathbf{x}}$ corresponds to the standard deviation of $\mathbf{x}$:

$$\bar{\mathbf{x}} = \frac{1}{2m} \sum_i k_i x_i \tag{4}$$

$$\sigma_{\mathbf{x}} = \sqrt{\frac{1}{2m} \sum_i k_i (x_i - \bar{\mathbf{x}})^2}. \tag{5}$$

k_i corresponds to the strength of node i.

Heterophilic mixing

The assortativity coefficient can also measure the heterophilic mixing between pairs of annotations. We define heterophilic mixing as the tendency for nodes with a given standardized scores for an attribute $\mathbf{x}$ to connect to nodes with similar standardized scores for another attribute $\mathbf{y}$. The assortativity coefficient, for pairs of annotations $\mathbf{x}$ and $\mathbf{y}$ is defined as:

$$r_{\mathbf{x},\mathbf{y}} = \sum_{ij} \frac{a_{ij}}{2m} \tilde{x_i} \tilde{y_j}, \tag{6}$$

Homophilic ratio

To quantify the extent to which individual regions connect to regions with similar attributes, we computed the homophilic ratio of each node. This measure is a ratio between the weighted average of the absolute difference of a node's annotation with its neighbors and the averaged absolute difference of this node's annotation with all the other nodes in the network. More precisely, the homophilic ratio h of a given node i for an annotation $\mathbf{x}$ is defined as

$$h_{\mathbf{x}}(i) = \frac{\sum_j \frac{a_{ij}}{k_i} |x_i - x_j|}{\frac{1}{n} \sum_j |x_i - x_j|}, \tag{7}$$

where n is the number of nodes in the connectome.

Mean connection distance

The mean homophilic ratio of each node was compared to its mean connection distance. This measure is defined as the average distance between a node and its connected neighbors, weighted by the weight of each connection. More precisely, the mean connection distance (MCD) of a node i is defined as

$$MCD(i) = \frac{1}{2m} \sum_j d_{ij} a_{ij}, \tag{8}$$

where d_{ij} corresponds to the Euclidean distance between nodes i and j.

Probabilistic activation maps

Using the Neurosynth meta-analytic engine [109] we extracted brain maps of probabilistic associations between functional key words and individual voxels, synthesized from results from more than 15,000 published fMRI studies. The probabilistic measures quantify the probability that a given term is reported in a study and that there is activation observed in a given voxel. It can be interpreted as a quantitative representation of how regional fluctuations in activity are related to psychological processes. We analyzed the functional maps associated to 123 cognitive and behavioural terms from the Cognitive Atlas ([70], ranging from umbrella terms ("attention", "emotion") to specific cognitive processes ("visual attention", "episodic memory"), behaviours ("eating", "sleep"), and emotional states ("fear", "anxiety").

Data and code availability

The data and code used to conduct the analyses presented in this paper are available at https://github.com/netneurolab/bazinet_assortativity.

ACKNOWLEDGMENTS

We thank Laura Suarez, Justine Hansen, Golia Shafiei, Bertha Vazquez-Rodriguez, Ross Markello, Zhen-Qi Liu, Filip Milisav and Andrea Luppi for insightful comments. VB acknowledges support from the Fonds du Recherche Québec - Nature et Technologies and from the Natural Sciences and Engineering Research Council of Canada (NSERC). BM acknowledges support from the NSERC, Canadian Institutes of Health Research (CIHR), Brain Canada Foundation Future Leaders Fund, the Canada Research Chairs Program, the Michael J. Fox Foundation, and the Healthy Brains for Healthy Lives initiative.

DECLARATION OF COMPETING INTERESTS

The authors declare no competing interests.

AUTHOR CONTRIBUTIONS

Conceptualization: V.B. and B.M.; Methodology: V.B. and B.M.; Formal Analysis: V.B.; Data Curation: V.B., J.Y.H., R.V., B.C.B.; Writing - Original Draft: V.B., B.M.; Writing - Review & Editing: J.Y.H., R.V., B.C.B., M.P.v.d.H.; Visualization: V.B.; Supervision: B.M.

[1] Akarca, D., Vértes, P. E., Bullmore, E. T., and Astle, D. E. (2021). A generative network model of neurodevelopmental diversity in structural brain organization. *Nature communications*, 12(1):1–18.

[2] Alexander-Bloch, A. F., Shou, H., Liu, S., Satterthwaite, T. D., Glahn, D. C., Shinohara, R. T., Vandekar, S. N., and Raznahan, A. (2018). On testing for spatial correspondence between maps of human brain structure and function. *Neuroimage*, 178:540–551.

[3] Amunts, K., Lepage, C., Borgeat, L., Mohlberg, H., Dickscheid, T., Rousseau, M.-É., Bludau, S., Bazin, P.-L., Lewis, L. B., Oros-Peusquens, A.-M., et al. (2013). Bigbrain: an ultrahigh-resolution 3d human brain model. *Science*, 340(6139):1472–1475.

[4] Arnatkeviciute, A., Fulcher, B. D., and Fornito, A. (2019). A practical guide to linking brain-wide gene expression and neuroimaging data. *Neuroimage*, 189:353–367.

[5] Arnatkeviciute, A., Fulcher, B. D., Pocock, R., and Fornito, A. (2018). Hub connectivity, neuronal diversity, and gene expression in the caenorhabditis elegans connectome. *PLoS Comput Biol*, 14(2):e1005989.

[6] Barbas, H. (1986). Pattern in the laminar origin of corticocortical connections. *Journal of Comparative Neurology*, 252(3):415–422.

[7] Barbas, H. and García-Cabezas, M. Á. (2016). How the prefrontal executive got its stripes. *Current Opinion in Neurobiology*, 40:125–134.

[8] Bassett, D. S., Brown, J. A., Deshpande, V., Carlson, J. M., and Grafton, S. T. (2011). Conserved and variable architecture of human white matter connectivity. *Neuroimage*, 54(2):1262–1279.

[9] Bassett, D. S., Bullmore, E., Verchinski, B. A., Mattay, V. S., Weinberger, D. R., and Meyer-Lindenberg, A. (2008). Hierarchical organization of human cortical networks in health and schizophrenia. *Journal of Neuroscience*, 28(37):9239–9248.

[10] Bazinet, V., de Wael, R. V., Hagmann, P., Bernhardt, B. C., and Misic, B. (2021). Multiscale communication in cortico-cortical networks. *NeuroImage*, 243:118546.

[11] Betzel, R. F. and Bassett, D. S. (2018). Specificity and robustness of long-distance connections in weighted, interareal connectomes. *Proceedings of the National Academy of Sciences*, 115(21):E4880–E4889.

[12] Betzel, R. F., Griffa, A., Hagmann, P., and Mišić, B. (2019). Distance-dependent consensus thresholds for generating group-representative structural brain networks. *Network neuroscience*, 3(2):475–496.

[13] Beul, S. F., Barbas, H., and Hilgetag, C. C. (2017). A predictive structural model of the primate connectome.

Scientific reports, 7(1):1–12.

[14] Beul, S. F. and Hilgetag, C. C. (2019). Neuron density fundamentally relates to architecture and connectivity of the primate cerebral cortex. *NeuroImage*, 189:777–792.

[15] Bijsterbosch, J., Harrison, S. J., Jbabdi, S., Woolrich, M., Beckmann, C., Smith, S., and Duff, E. P. (2020). Challenges and future directions for representations of functional brain organization. *Nature neuroscience*, 23(12):1484–1495.

[16] Bullmore, E. and Sporns, O. (2009). Complex brain networks: graph theoretical analysis of structural and functional systems. *Nature reviews neuroscience*, 10(3):186–198.

[17] Bullmore, E. and Sporns, O. (2012). The economy of brain network organization. *Nature Reviews Neuroscience*, 13(5):336–349.

[18] Burt, J. B., Demirtaş, M., Eckner, W. J., Navejar, N. M., Ji, J. L., Martin, W. J., Bernacchia, A., Anticevic, A., and Murray, J. D. (2018). Hierarchy of transcriptomic specialization across human cortex captured by structural neuroimaging topography. *Nature neuroscience*, 21(9):1251–1259.

[19] Burt, J. B., Helmer, M., Shinn, M., Anticevic, A., and Murray, J. D. (2020). Generative modeling of brain maps with spatial autocorrelation. *NeuroImage*, 220:117038.

[20] Cammoun, L., Gigandet, X., Meskaldji, D., Thiran, J. P., Sporns, O., Do, K. Q., Maeder, P., Meuli, R., and Hagmann, P. (2012). Mapping the human connectome at multiple scales with diffusion spectrum MRI. *Journal of Neuroscience Methods*, 203(2):386–397.

[21] Collins, C. E., Airey, D. C., Young, N. A., Leitch, D. B., and Kaas, J. H. (2010). Neuron densities vary across and within cortical areas in primates. *Proceedings of the National Academy of Sciences*, 107(36):15927–15932.

[22] Daducci, A., Gerhard, S., Griffa, A., Lemkaddem, A., Cammoun, L., Gigandet, X., Meuli, R., Hagmann, P., and Thiran, J.-P. (2012). The connectome mapper: an open-source processing pipeline to map connectomes with mri. *PloS one*, 7(12):e48121.

[23] Desikan, R. S., Ségonne, F., Fischl, B., Quinn, B. T., Dickerson, B. C., Blacker, D., Buckner, R. L., Dale, A. M., Maguire, R. P., Hyman, B. T., Albert, M. S., and Killiany, R. J. (2006). An automated labeling system for subdividing the human cerebral cortex on MRI scans into gyral based regions of interest. *NeuroImage*, 31(3):968–980.

[24] Dhollander, T., Raffelt, D., and Connelly, A. (2016). Unsupervised 3-tissue response function estimation from single-shell or multi-shell diffusion mr data without a co-registered t1 image. In *ISMRM Workshop on Breaking the Barriers of Diffusion MRI*, volume 5, page 5.

[25] Donahue, C. J., Sotiropoulos, S. N., Jbabdi, S., Hernandez-Fernandez, M., Behrens, T. E., Dyrby, T. B., Coalson, T., Kennedy, H., Knoblauch, K., Van Essen, D. C., et al. (2016). Using diffusion tractography to predict cortical connection strength and distance: a quantitative comparison with tracers in the monkey. *Journal of Neuroscience*, 36(25):6758–6770.

[26] Eickhoff, S. B., Yeo, B., and Genon, S. (2018). Imaging-based parcellations of the human brain. *Nature Reviews Neuroscience*, 19(11):672–686.

[27] Ercsey-Ravasz, M., Markov, N. T., Lamy, C., Van Essen, D. C., Knoblauch, K., Toroczkai, Z., and Kennedy, H. (2013). A predictive network model of cerebral cortical connectivity based on a distance rule. *Neuron*, 80(1):184–197.

[28] Fornito, A., Arnatkevičiūtė, A., and Fulcher, B. D. (2019). Bridging the gap between connectome and transcriptome. *Trends in Cognitive Sciences*, 23(1):34–50.

[29] French, L. and Pavlidis, P. (2011). Relationships between gene expression and brain wiring in the adult rodent brain. *PLoS computational biology*, 7(1):e1001049.

[30] Froudist-Walsh, S., Xu, T., Niu, M., Rapan, L., Margulies, D. S., Zilles, K., Wang, X.-J., and Palomero-Gallagher, N. (2021). Gradients of receptor expression in the macaque cortex. *bioRxiv*.

[31] Fulcher, B. D., Arnatkeviciute, A., and Fornito, A. (2021). Overcoming false-positive gene-category enrichment in the analysis of spatially resolved transcriptomic brain atlas data. *Nature communications*, 12(1):1–13.

[32] Fulcher, B. D. and Fornito, A. (2016). A transcriptional signature of hub connectivity in the mouse connectome. *Proceedings of the National Academy of Sciences*, 113(5):1435–1440.

[33] Fulcher, B. D., Murray, J. D., Zerbi, V., and Wang, X.-J. (2019). Multimodal gradients across mouse cortex. *Proceedings of the National Academy of Sciences*, 116(10):4689–4695.

[34] García-Cabezas, M. Á., Zikopoulos, B., and Barbas, H. (2019). The structural model: a theory linking connections, plasticity, pathology, development and evolution of the cerebral cortex. *Brain Structure and Function*, 224(3):985–1008.

[35] Glasser, M. F., Sotiropoulos, S. N., Wilson, J. A., Coalson, T. S., Fischl, B., Andersson, J. L., Xu, J., Jbabdi, S., Webster, M., Polimeni, J. R., et al. (2013). The minimal preprocessing pipelines for the human connectome project. *Neuroimage*, 80:105–124.

[36] Glasser, M. F. and Van Essen, D. C. (2011). Mapping human cortical areas in vivo based on myelin content as revealed by t1-and t2-weighted mri. *Journal of Neuroscience*, 31(32):11597–11616.

[37] Goulas, A., Betzel, R. F., and Hilgetag, C. C. (2019). Spatiotemporal ontogeny of brain wiring. *Science advances*, 5(6):eaav9694.

[38] Goulas, A., Changeux, J.-P., Wagstyl, K., Amunts, K., Palomero-Gallagher, N., and Hilgetag, C. C. (2021). The natural axis of transmitter receptor distribution in the human cerebral cortex. *Proceedings of the National Academy of Sciences*, 118(3).

[39] Goulas, A., Zilles, K., and Hilgetag, C. C. (2018). Cortical gradients and laminar projections in mammals. *Trends in Neurosciences*, 41(11):775–788.

[40] Griffa, A., Alemán-Gómez, Y., and Hagmann, P. (2019). Structural and functional connectome from 70 young healthy adults. doi:10.5281/zenodo.2872624. type: dataset.

[41] Hagmann, P., Cammoun, L., Gigandet, X., Meuli, R., Honey, C. J., Wedeen, V. J., and Sporns, O. (2008). Mapping the structural core of human cerebral cortex. *PLoS biology*, 6(7):e159.

[42] Hansen, J. Y., Shafiei, G., Markello, R. D., Smart, K., Cox, S. M., Wu, Y., Gallezot, J.-D., Aumont, É., Servaes, S., Scala, S. G., et al. (2021). Mapping neurotransmitter systems to the structural and functional organization of the human neocortex. *bioRxiv*.

[43] Hawrylycz, M. J., Lein, E. S., Guillozet-Bongaarts, A. L., Shen, E. H., Ng, L., Miller, J. A., Van De Lagemaat, L. N., Smith, K. A., Ebbert, A., Riley, Z. L., et al. (2012). An

anatomically comprehensive atlas of the adult human brain transcriptome. *Nature*, 489(7416):391–399.

[44] Hilgetag, C. C., Beul, S. F., van Albada, S. J., and Goulas, A. (2019). An architectonic type principle integrates macroscopic cortico-cortical connections with intrinsic cortical circuits of the primate brain. *Network neuroscience*, 3(4):905–923.

[45] Hilgetag, C. C. and Goulas, A. (2020). 'hierarchy'in the organization of brain networks. *Philosophical Transactions of the Royal Society B*, 375(1796):20190319.

[46] Horvát, S., Gămănuț, R., Ercsey-Ravasz, M., Magrou, L., Gămănuț, B., Van Essen, D. C., Burkhalter, A., Knoblauch, K., Toroczkai, Z., and Kennedy, H. (2016). Spatial embedding and wiring cost constrain the functional layout of the cortical network of rodents and primates. *PLoS Biol*, 14(7):e1002512.

[47] Huntenburg, J. M., Bazin, P.-L., Goulas, A., Tardif, C. L., Villringer, A., and Margulies, D. S. (2017). A systematic relationship between functional connectivity and intracortical myelin in the human cerebral cortex. *Cerebral Cortex*, 27(2):981–997.

[48] Huntenburg, J. M., Bazin, P.-L., and Margulies, D. S. (2018). Large-scale gradients in human cortical organization. *Trends in cognitive sciences*, 22(1):21–31.

[49] Jeurissen, B., Tournier, J.-D., Dhollander, T., Connelly, A., and Sijbers, J. (2014). Multi-tissue constrained spherical deconvolution for improved analysis of multi-shell diffusion mri data. *NeuroImage*, 103:411–426.

[50] Krienen, F. M., Yeo, B. T., Ge, T., Buckner, R. L., and Sherwood, C. C. (2016). Transcriptional profiles of supragranular-enriched genes associate with corticocortical network architecture in the human brain. *Proceedings of the National Academy of Sciences*, 113(4):E469–E478.

[51] Lariviere, S., Vos de Wael, R., Paquola, C., Hong, S.-J., Mišić, B., Bernasconi, N., Bernasconi, A., Bonilha, L., and Bernhardt, B. C. (2019). Microstructure-informed connectomics: enriching large-scale descriptions of healthy and diseased brains. *Brain connectivity*, 9(2):113–127.

[52] Lein, E. S., Hawrylycz, M. J., Ao, N., Ayres, M., Bensinger, A., Bernard, A., Boe, A. F., Boguski, M. S., Brockway, K. S., Byrnes, E. J., et al. (2007). Genome-wide atlas of gene expression in the adult mouse brain. *Nature*, 445(7124):168–176.

[53] Liu, Z.-Q., Vázquez-Rodríguez, B., Spreng, R. N., Bernhardt, B. C., Betzel, R. F., and Misic, B. (2022). Time-resolved structure-function coupling in brain networks. *Communications Biology*.

[54] Maier-Hein, K. H., Neher, P. F., Houde, J.-C., Côté, M.-A., Garyfallidis, E., Zhong, J., Chamberland, M., Yeh, F.-C., Lin, Y.-C., Ji, Q., et al. (2017). The challenge of mapping the human connectome based on diffusion tractography. *Nature communications*, 8(1):1–13.

[55] Margulies, D. S., Ghosh, S. S., Goulas, A., Falkiewicz, M., Huntenburg, J. M., Langs, G., Bezgin, G., Eickhoff, S. B., Castellanos, F. X., Petrides, M., et al. (2016). Situating the default-mode network along a principal gradient of macroscale cortical organization. *Proceedings of the National Academy of Sciences*, 113(44):12574–12579.

[56] Markello, R. D., Arnatkeviciute, A., Poline, J.-B., Fulcher, B. D., Fornito, A., and Misic, B. (2021). Standardizing workflows in imaging transcriptomics with the abagen toolbox. *Elife*, 10:e72129.

[57] Markello, R. D., Hansen, J. Y., Liu, Z.-Q., Bazinet, V., Shafiei, G., Suarez, L. E., Blostein, N., Seidlitz, J., Baillet, S., Satterthwaite, T. D., et al. (2022). Neuromaps: structural and functional interpretation of brain maps. *bioRxiv*.

[58] Markello, R. D. and Misic, B. (2021). Comparing spatial null models for brain maps. *NeuroImage*, 236:118052.

[59] Mesulam, M.-M. (1998). From sensation to cognition. *Brain: a journal of neurology*, 121(6):1013–1052.

[60] Mišić, B., Betzel, R. F., Nematzadeh, A., Goni, J., Griffa, A., Hagmann, P., Flammini, A., Ahn, Y.-Y., and Sporns, O. (2015). Cooperative and competitive spreading dynamics on the human connectome. *Neuron*, 86(6):1518–1529.

[61] Mišić, B., Fatima, Z., Askren, M. K., Buschkuehl, M., Churchill, N., Cimprich, B., Deldin, P. J., Jaeggi, S., Jung, M., Korostil, M., et al. (2014a). The functional connectivity landscape of the human brain. *PLoS ONE*, 9(10):e111007.

[62] Mišić, B., Goñi, J., Betzel, R. F., Sporns, O., and McIntosh, A. R. (2014b). A network convergence zone in the hippocampus. *PLoS Comput Biol*, 10(12):e1003982.

[63] Newman, M. E. (2003). Mixing patterns in networks. *Physical review E*, 67(2):026126.

[64] Oh, S. W., Harris, J. A., Ng, L., Winslow, B., Cain, N., Mihalas, S., Wang, Q., Lau, C., Kuan, L., Henry, A. M., et al. (2014). A mesoscale connectome of the mouse brain. *Nature*, 508(7495):207–214.

[65] Oldham, S., Fulcher, B. D., Aquino, K. M., Arnatkeviciute, A. M., Paquola, C., Shishegar, R., and Fornito, A. (2021). Modeling spatial, developmental, physiological, and topological constraints on human brain connectivity. *bioRxiv*.

[66] Palomero-Gallagher, N., Amunts, K., and Zilles, K. (2015). Transmitter receptor distribution in the human brain. In *Brain Mapping*, pages 261–275. Elsevier.

[67] Paquola, C., Vos De Wael, R., Wagstyl, K., Bethlehem, R. A., Hong, S.-J., Seidlitz, J., Bullmore, E. T., Evans, A. C., Misic, B., Margulies, D. S., et al. (2019). Microstructural and functional gradients are increasingly dissociated in transmodal cortices. *PLoS biology*, 17(5):e3000284.

[68] Park, B.-y., de Wael, R. V., Paquola, C., Larivière, S., Benkarim, O., Royer, J., Tavakol, S., Cruces, R. R., Li, Q., Valk, S. L., et al. (2021). Signal diffusion along connectome gradients and inter-hub routing differentially contribute to dynamic human brain function. *NeuroImage*, page 117429.

[69] Passingham, R. E., Stephan, K. E., and Kötter, R. (2002). The anatomical basis of functional localization in the cortex. *Nature Reviews Neuroscience*, 3(8):606–616.

[70] Poldrack, R. A., Kittur, A., Kalar, D., Miller, E., Seppa, C., Gil, Y., Parker, D. S., Sabb, F. W., and Bilder, R. M. (2011). The cognitive atlas: toward a knowledge foundation for cognitive neuroscience. *Frontiers in neuroinformatics*, 5:17.

[71] Power, J. D., Barnes, K. A., Snyder, A. Z., Schlaggar, B. L., and Petersen, S. E. (2012). Spurious but systematic correlations in functional connectivity mri networks arise from subject motion. *Neuroimage*, 59(3):2142–2154.

[72] Power, J. D., Cohen, A. L., Nelson, S. M., Wig, G. S., Barnes, K. A., Church, J. A., Vogel, A. C., Laumann, T. O., Miezin, F. M., Schlaggar, B. L., et al. (2011). Functional network organization of the human brain. *Neuron*,

72(4):665–678.

[73] Richiardi, J., Altmann, A., Milazzo, A.-C., Chang, C., Chakravarty, M. M., Banaschewski, T., Barker, G. J., Bokde, A. L., Bromberg, U., Büchel, C., et al. (2015). Correlated gene expression supports synchronous activity in brain networks. *Science*, 348(6240):1241–1244.

[74] Roberts, J. A., Perry, A., Lord, A. R., Roberts, G., Mitchell, P. B., Smith, R. E., Calamante, F., and Breakspear, M. (2016). The contribution of geometry to the human connectome. *Neuroimage*, 124:379–393.

[75] Rockland, K. S. and Pandya, D. N. (1979). Laminar origins and terminations of cortical connections of the occipital lobe in the rhesus monkey. *Brain research*, 179(1):3–20.

[76] Schaefer, A., Kong, R., Gordon, E. M., Laumann, T. O., Zuo, X.-N., Holmes, A. J., Eickhoff, S. B., and Yeo, B. T. (2018). Local-global parcellation of the human cerebral cortex from intrinsic functional connectivity mri. *Cerebral cortex*, 28(9):3095–3114.

[77] Scholtens, L. H., Schmidt, R., de Reus, M. A., and van den Heuvel, M. P. (2014). Linking macroscale graph analytical organization to microscale neuroarchitectonics in the macaque connectome. *Journal of Neuroscience*, 34(36):12192–12205.

[78] Seidlitz, J., Nadig, A., Liu, S., Bethlehem, R. A., Vértes, P. E., Morgan, S. E., Váša, F., Romero-Garcia, R., Lalonde, F. M., Clasen, L. S., et al. (2020). Transcriptomic and cellular decoding of regional brain vulnerability to neurogenetic disorders. *Nature communications*, 11(1):1–14.

[79] Sepulcre, J., Liu, H., Talukdar, T., Martincorena, I., Yeo, B. T., and Buckner, R. L. (2010). The organization of local and distant functional connectivity in the human brain. *PLoS computational biology*, 6(6):e1000808.

[80] Shafiei, G., Markello, R. D., De Wael, R. V., Bernhardt, B. C., Fulcher, B. D., and Misic, B. (2020). Topographic gradients of intrinsic dynamics across neocortex. *Elife*, 9:e62116.

[81] Shine, J. M. (2019). Neuromodulatory influences on integration and segregation in the brain. *Trends in cognitive sciences*, 23(7):572–583.

[82] Smith, R. E., Tournier, J.-D., Calamante, F., and Connelly, A. (2015). Sift2: Enabling dense quantitative assessment of brain white matter connectivity using streamlines tractography. *Neuroimage*, 119:338–351.

[83] Sporns, O. (2013). Network attributes for segregation and integration in the human brain. *Current opinion in neurobiology*, 23(2):162–171.

[84] Sporns, O. and Betzel, R. F. (2016). Modular brain networks. *Annual review of psychology*, 67:613–640.

[85] Stephan, K. E., Hilgetag, C.-C., Burns, G. A., O'Neill, M. A., Young, M. P., and Kotter, R. (2000). Computational analysis of functional connectivity between areas of primate cerebral cortex. *Philosophical Transactions of the Royal Society of London. Series B: Biological Sciences*, 355(1393):111–126.

[86] Stephan, K. E., Kamper, L., Bozkurt, A., Burns, G. A., Young, M. P., and Kötter, R. (2001). Advanced database methodology for the collation of connectivity data on the macaque brain (cocomac). *Philosophical Transactions of the Royal Society of London. Series B: Biological Sciences*, 356(1412):1159–1186.

[87] Stiso, J. and Bassett, D. S. (2018). Spatial embedding imposes constraints on neuronal network architectures. *Trends in cognitive sciences*, 22(12):1127–1142.

[88] Suárez, L. E., Markello, R. D., Betzel, R. F., and Misic, B. (2020). Linking structure and function in macroscale brain networks. *Trends in Cognitive Sciences*, 24(4):302–315.

[89] Sydnor, V. J., Larsen, B., Bassett, D. S., Alexander-Bloch, A., Fair, D. A., Liston, C., Mackey, A. P., Milham, M. P., Pines, A., Roalf, D. R., et al. (2021). Neurodevelopment of the association cortices: Patterns, mechanisms, and implications for psychopathology. *Neuron*, 109(18):2820–2846.

[90] Thomas, C., Frank, Q. Y., Irfanoglu, M. O., Modi, P., Saleem, K. S., Leopold, D. A., and Pierpaoli, C. (2014). Anatomical accuracy of brain connections derived from diffusion mri tractography is inherently limited. *Proceedings of the National Academy of Sciences*, 111(46):16574–16579.

[91] Tournier, J.-D., Smith, R., Raffelt, D., Tabbara, R., Dhollander, T., Pietsch, M., Christiaens, D., Jeurissen, B., Yeh, C.-H., and Connelly, A. (2019). Mrtrix3: A fast, flexible and open software framework for medical image processing and visualisation. *NeuroImage*, 202:116137.

[92] Van den Heuvel, M. P., Bullmore, E. T., and Sporns, O. (2016). Comparative connectomics. *Trends in cognitive sciences*, 20(5):345–361.

[93] van den Heuvel, M. P., de Reus, M. A., Barrett, L. F., Scholtens, L. H., Coopmans, F. M., Schmidt, R., Preuss, T. M., Rilling, J. K., and Li, L. (2015a). Comparison of diffusion tractography and tract-tracing measures of connectivity strength in rhesus macaque connectome. *Human Brain Mapping*, 36(8):3064–3075.

[94] Van Den Heuvel, M. P., Kahn, R. S., Goñi, J., and Sporns, O. (2012). High-cost, high-capacity backbone for global brain communication. *Proceedings of the National Academy of Sciences*, 109(28):11372–11377.

[95] van den Heuvel, M. P., Scholtens, L. H., Barrett, L. F., Hilgetag, C. C., and de Reus, M. A. (2015b). Bridging cytoarchitectonics and connectomics in human cerebral cortex. *Journal of Neuroscience*, 35(41):13943–13948.

[96] Van Den Heuvel, M. P. and Sporns, O. (2011). Rich-club organization of the human connectome. *Journal of Neuroscience*, 31(44):15775–15786.

[97] Van Essen, D. C., Smith, J., Glasser, M. F., Elam, J., Donahue, C. J., Dierker, D. L., Reid, E. K., Coalson, T., and Harwell, J. (2017). The brain analysis library of spatial maps and atlases (balsa) database. *Neuroimage*, 144:270–274.

[98] Van Essen, D. C., Smith, S. M., Barch, D. M., Behrens, T. E. J., Yacoub, E., and Ugurbil, K. (2013). The WU-minn human connectome project: An overview. *NeuroImage*, 80:62–79.

[99] Vasa, F. and Misic, B. (2022). Null models in network neuroscience. *Nat Rev Neurosci*.

[100] Vázquez-Rodríguez, B., Suárez, L. E., Markello, R. D., Shafiei, G., Paquola, C., Hagmann, P., Van Den Heuvel, M. P., Bernhardt, B. C., Spreng, R. N., and Misic, B. (2019). Gradients of structure–function tethering across neocortex. *Proceedings of the National Academy of Sciences*, 116(42):21219–21227.

[101] Vértes, P. E., Rittman, T., Whitaker, K. J., Romero-Garcia, R., Váša, F., Kitzbichler, M. G., Wagstyl, K., Fonagy, P., Dolan, R. J., Jones, P. B., et al. (2016). Gene transcription profiles associated with inter-modular hubs and connection distance in human

functional magnetic resonance imaging networks. *Philosophical Transactions of the Royal Society B: Biological Sciences*, 371(1705):20150362.

[102] Vézquez-Rodríguez, B., Liu, Z.-Q., Hagmann, P., and Misic, B. (2020). Signal propagation via cortical hierarchies. *Network Neuroscience*, 4(4):1072–1090.

[103] Vos de Wael, R., Benkarim, O., Paquola, C., Lariviere, S., Royer, J., Tavakol, S., Xu, T., Hong, S.-J., Langs, G., Valk, S., et al. (2020). Brainspace: a toolbox for the analysis of macroscale gradients in neuroimaging and connectomics datasets. *Communications biology*, 3(1):1–10.

[104] Wagner, H. H. and Dray, S. (2015). Generating spatially constrained null models for irregularly spaced data using m oran spectral randomization methods. *Methods in Ecology and Evolution*, 6(10):1169–1178.

[105] Wagstyl, K., Larocque, S., Cucurull, G., Lepage, C., Cohen, J. P., Bludau, S., Palomero-Gallagher, N., Lewis, L. B., Funck, T., Spitzer, H., et al. (2020). Bigbrain 3d atlas of cortical layers: cortical and laminar thickness gradients diverge in sensory and motor cortices. *PLoS biology*, 18(4):e3000678.

[106] Wang, Y., Royer, J., Park, B.-y., Vos de Wael, R., Larivière, S., Tavakol, S., Rodriguez-Cruces, R., Paquola, C., Hong, S.-J., Margulies, D. S., et al. (2022). Long-range functional connections mirror and link microarchitectural and cognitive hierarchies in the human brain. *Cerebral Cortex*.

[107] Wei, Y., Scholtens, L. H., Turk, E., and Van Den Heuvel, M. P. (2018). Multiscale examination of cytoarchitectonic similarity and human brain connectivity. *Network Neuroscience*, 3(1):124–137.

[108] Weiskopf, N., Mohammadi, S., Lutti, A., and Callaghan, M. F. (2015). Advances in mri-based computational neuroanatomy: from morphometry to in-vivo histology. *Current opinion in neurology*, 28(4):313–322.

[109] Yarkoni, T., Poldrack, R. A., Nichols, T. E., Van Essen, D. C., and Wager, T. D. (2011). Large-scale automated synthesis of human functional neuroimaging data. *Nature methods*, 8(8):665–670.

[110] Yeo, B. T., Krienen, F. M., Sepulcre, J., Sabuncu, M. R., Lashkari, D., Hollinshead, M., Roffman, J. L., Smoller, J. W., Zöllei, L., Polimeni, J. R., et al. (2011). The organization of the human cerebral cortex estimated by intrinsic functional connectivity. *Journal of neurophysiology*.

[111] Zilles, K. and Palomero-Gallagher, N. (2017). Multiple transmitter receptors in regions and layers of the human cerebral cortex. *Frontiers in neuroanatomy*, 11:78.

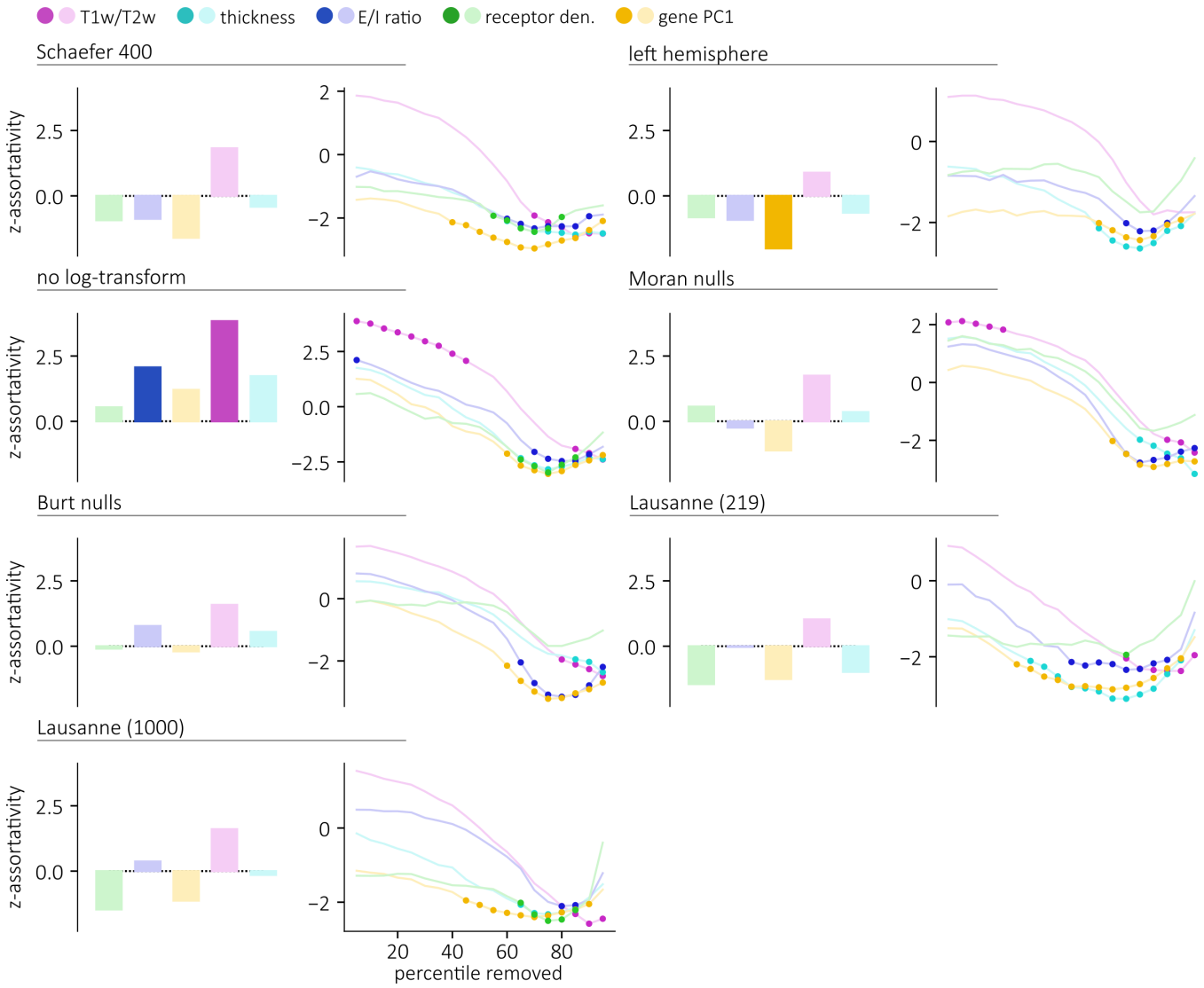

Figure S1. **Sensitivity and replication (homophilic mixing) |** To ensure that the results obtained in the structural connectome are not sensitive to our processing choices, we replicated our experiments using the 400 nodes Schaefer parcellation, using the left-hemisphere connectome, using edge weights that were not log-transformed, using Moran nulls and Burt nulls instead of the spin nulls and using an additional independently-acquired dataset, parcellated at a low- (219 nodes) and high-resolution (1000 nodes). For each sensitivity and replication experiment, and for each annotations, we re-computed the standardized assortativity scores (left). We also re-computed the standardized assortativity across thresholded connectomes where a given percentile of the shortest connections are removed (right).

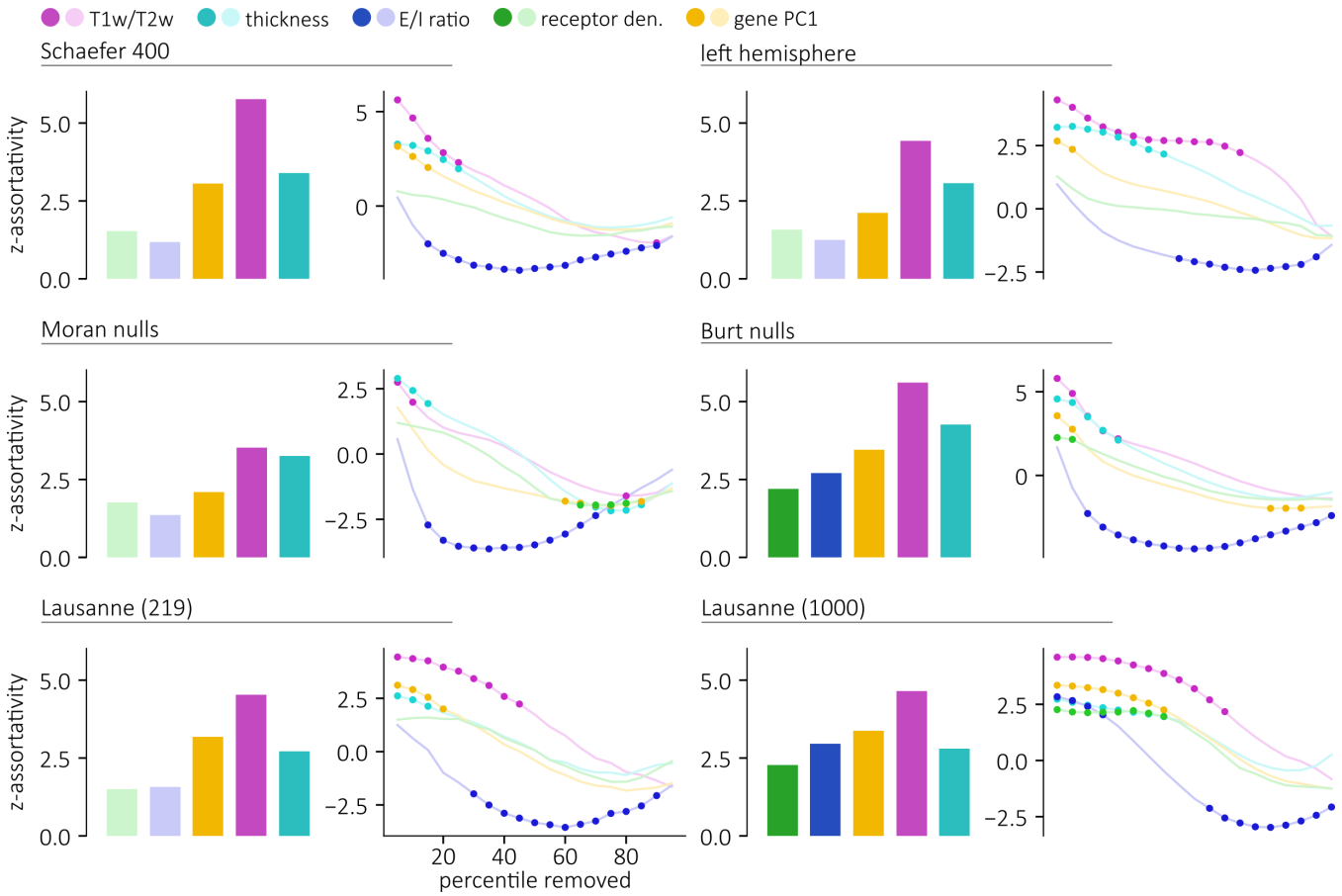

Figure S2. **Sensitivity and replication (homophilic mixing) |** To ensure that the results obtained in the functional connectome are not sensitive to our processing choices, we replicated our experiments using the 400 nodes Schaefer parcellation, using the left-hemisphere connectome, using Moran nulls and Burt nulls instead of the spin nulls, and using an additional independently-acquired dataset parcellated at a low- (219 nodes) and high-resolution (1000 nodes). For each sensitivity and replication experiment, and each annotations, we re-computed the standardized assortativity scores (left). We also re-computed the standardized assortativity across thresholded connectomes where a given percentile of the shortest connections are removed (right).

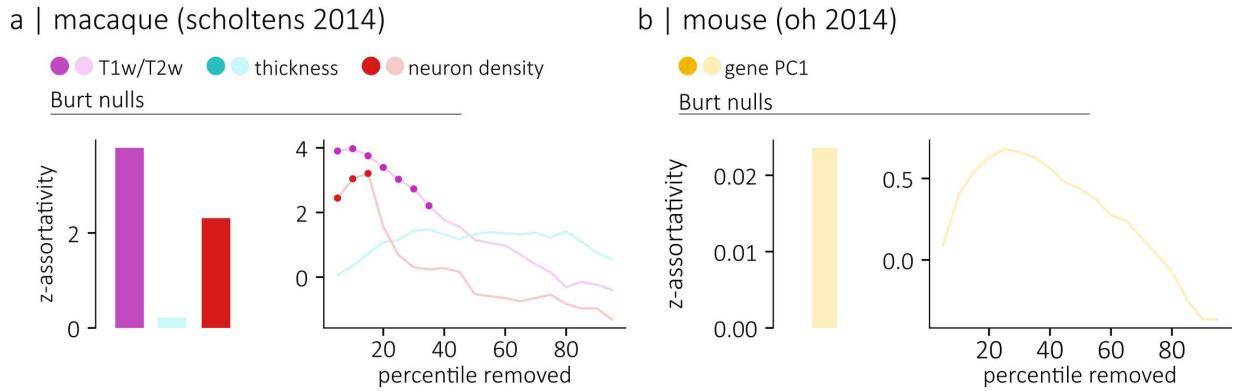

Figure S3. **Sensitivity and replication (homophilic mixing) |** To ensure that the results obtained in the animal connectomes are not sensitive to the spatial autocorrelation-preserving null model used, we replicated our experiments using Burt nulls. For each sensitivity and replication experiment, and for each annotations, we re-computed the standardized assortativity scores (left). We also re-computed the standardized assortativity across thresholded connectomes where a given percentile of the shortest connections are removed (right).

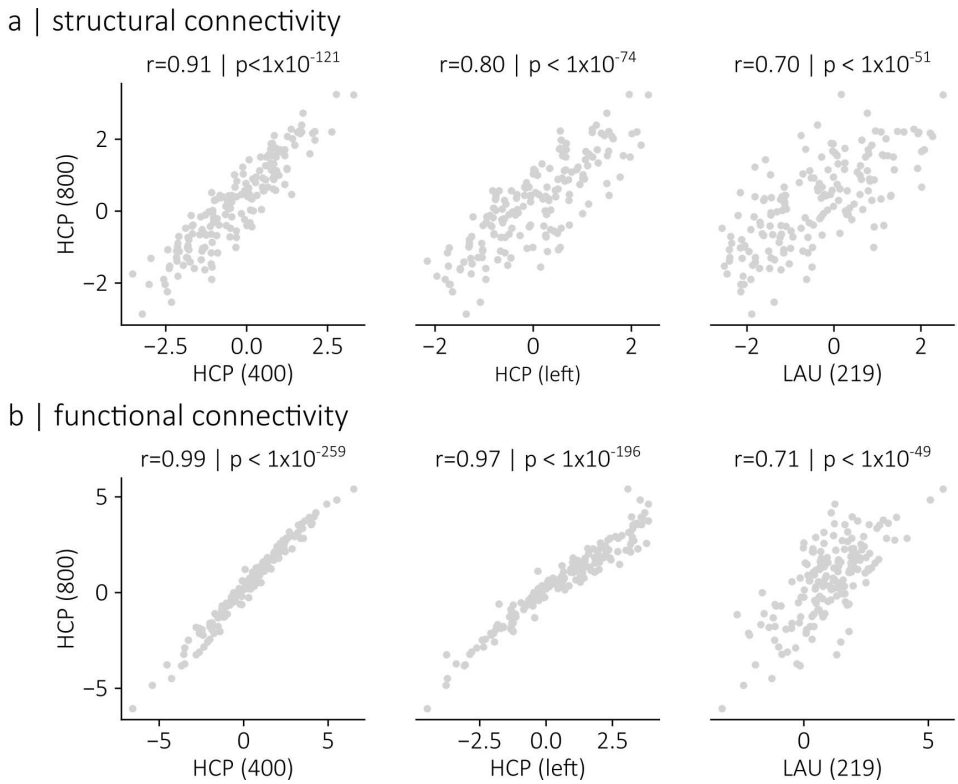

Figure S4. **Sensitivity and replication (heterophilic mixing) |** To ensure that the heterophilic relationships of receptors and transporters uncovered in Fig. 5 are replicable, we correlated the z-assortativity scores presented in Fig. 5, which were obtained using the HCP dataset and the Schaefer 800-nodes parcellation, with the z-assortativity scores obtained using an alternate parcellation namely, the 400-nodes Schaefer parcellation (right). We also correlated the z-assortativity scores presented in Fig. 5 with z-assortativity scores obtained when considering only the left-hemisphere nodes of the connectome (middle), and when using an alternate dataset and parcellation, namely the Lausanne dataset and the 219-nodes Cammoun parcellation (left). Scatterplots of the correlations are presented for the human structural connectome (a) and for the human functional connectome (b). We find significant correlations for all sensitivity and replication experiments.

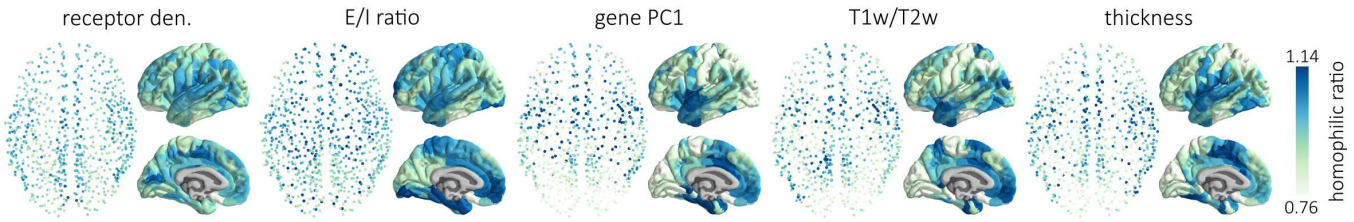

Figure S5. **Homophilic ratios in the functional connectome |** Homophilic ratios are shown for the human functional connectome. Micro-architectural attributes include the density of neurotransmitter receptors, the ratio of excitatory/inhibitory receptors, the principal axis of gene transcription variation, the T1w/T2w ratio and cortical thickness.

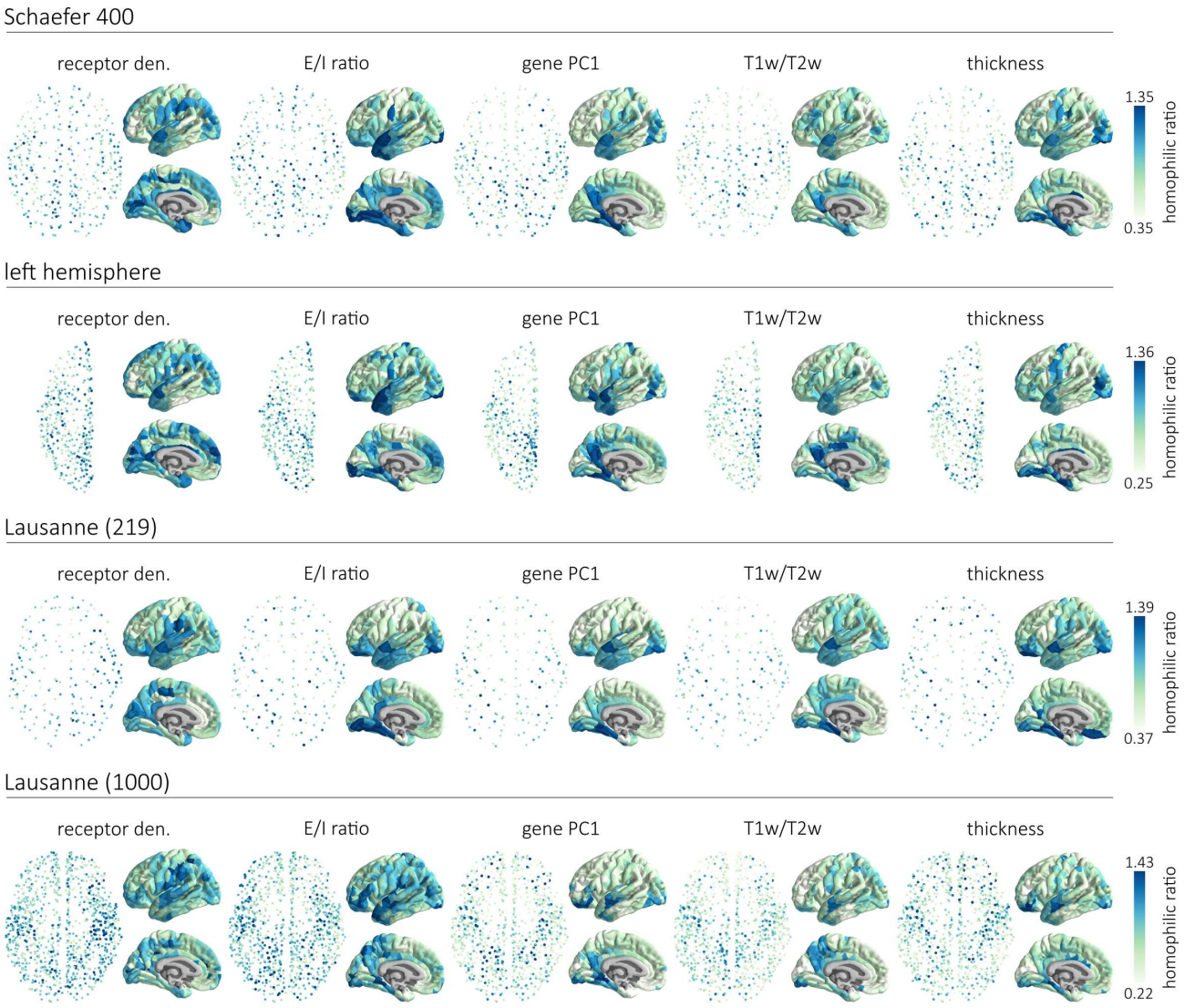

Figure S6. **Sensitivity and replication (homophilic ratios) |** To ensure that our results are not confounded by processing choices, we computed the homophilic ratios of each micro-architectural attribute in a structural connectome generated using the 400 nodes Schaefer parcellation, in a structural connectome of the brain's left-hemisphere, and in a structural connectome reconstructed using an independently acquired diffusion imaging dataset and parcellated into 219 and 1000 brain regions. The micro-architectural attributes include the density of neurotransmitter receptors, the ratio of excitatory/inhibitory receptors, the principal axis of gene transcription variation, the T1w/T2w ratio and cortical thickness.